

**INSTRUMENTATION AND CALIBRATION OF X-RAY
SCINTILLATION PAIR SPECTROMETER**

Joseph Edward Synder, Jr.

Library
U. S. Naval Postgraduate School
Monterey, California

25222

INSTRUMENTATION AND CALIBRATION OF
X-RAY SCINTILLATION PAIR SPECTROMETER

by

Joseph Edward Snyder, Jr.
B.S., United States Naval Academy
(1944)

Submitted in Partial Fulfillment of the
Requirements for the Degree of

MASTER OF SCIENCE

at the

MASSACHUSETTS INSTITUTE OF TECHNOLOGY
(1955)

Signature of Author _____ Department of Physics, May 23, 1955

Certified by _____ Thesis Supervisor

Accepted by _____ Chairman, Departmental Committee on Graduate Students

INSTRUMENTATION AND CALIBRATION OF
X-RAY SCINTILLATION PAIR SPECTROMETER

by

Joseph Edward Snyder, Jr.
U.S. Navy, United States Naval Academy
(1951)

Submitted in Partial Fulfillment of the
Requirements for the Degree of

MASTER OF SCIENCE

at the

MASSACHUSETTS INSTITUTE OF TECHNOLOGY
(1952)

Signature of Author
Department of Physics, May 23, 1952

Certified by
Thesis Supervisor

Accepted by
Chairman, Departmental Committee on Graduate Students

INSTRUMENTATION AND CALIBRATION OF
X-RAY SCINTILLATION PAIR SPECTROMETER

by

Joseph Edward Snyder, Jr.

Submitted to the Department of Physics on May 23, 1955 in partial fulfillment of the requirements for the degree of Master of Science.

ABSTRACT

This paper describes an x-ray spectrometer designed for use at the M.I.T. linear accelerator. The spectrometer is a three-counter telescope with a thin lead radiator between the first and second counter. The first and second counters are thin plastic scintillators; the third, a thick plastic scintillator. An acceptable event is one in which there is no pulse in the first counter and a doubly ionizing pulse in the second counter in coincidence with the third counter. Such events should be electron-positron pairs originating only in the radiator. To a first approximation, the sum of the pulse heights produced in the second and third counter is proportional to the incident x-ray energy.

Thesis Supervisor: Bernard T. Feld

Title: Associate Professor of Physics

INVESTIGATION AND CALIBRATION OF
X-RAY SCINTILLATION PULSE SPECTROMETER

by

Joseph Edward Snyder, Jr.

Submitted to the Department of Physics on May 22, 1952 in partial fulfillment of the requirements for the degree of Master of Science.

1952

This report describes an x-ray spectrometer designed for use as the M.I.T. linear accelerator. The spectrometer is a three-counter telescope with a thin lead radiator between the first and second counters. The first and second counters are thin plastic scintillators; the third, a thick plastic scintillator. An adjustable event is one in which there is no pulse in the first counter and a doubly ionizing pulse in the second counter in coincidence with the third counter. Such events should be electron-positron pairs originating only in the radiator. To a first approximation, the sum of the pulse heights produced in the second and third counter is proportional to the incident x-ray energy.

Thesis Supervisor: Bernard T. Feld

Title: Associate Professor of Physics

TABLE OF CONTENTS

	Page Number
I. INTRODUCTION	1
II. APPARATUS	6
DESCRIPTION OF SPECTROMETER	6
ELECTRONIC CIRCUIT	10
III. SELECTION OF PAIRS	19
IV. FUNCTION OF SCINTILLATOR NO. 3	23
V. RESOLUTION	24
LIGHT COLLECTION AND PHOTOMULTIPLIER STATISTICS	24
RADIATION ENERGY LOSS	25
ELECTRON ESCAPE	26
ENERGY LOSS IN THE CONVERTER	28
CAPTURE OF ANNIHILATION QUANTA	30
SUMMARY OF EXPECTED RESOLUTION	31
VI. CALIBRATION AT THE ROCKEFELLER ELECTROSTATIC GENERATOR	32
VII. DISCUSSION OF EXPERIMENTAL RESULTS	36
ENERGY CALIBRATION	36
FLUORINE RUNS	40
HIGH-ENERGY RUNS	45
VIII. SUMMARY	47
APPENDIX I. CALCULATION OF DIFFERENTIAL ENERGY LOSS DISTRIBUTION FOR SCINTILLATOR NO. 2 AT 17.6 Mev INCIDENT X-RAY ENERGY	48
Bibliography	51

TABLE OF CONTENTS

Page Number

1	I. INTRODUCTION
6	II. APPARATUS
6	DESCRIPTION OF SCINTILLATOR
10	ABSTRACTED CIRCUIT
19	III. SELECTION OF PAIR
23	IV. EXHIBITION OF SCINTILLATION NO. 3
24	V. RESOLUTION
24	LIGHT COLLECTION AND PHOTOGRAPHIC STATISTICS
25	RADIATION ENERGY LOSS
26	KINETIC ENERGY
28	ENERGY LOSS IN THE CONVERTER
30	CAUTIONS ON AMPLIFICATION QUANTA
31	SUMMARY OF EXPECTED RESOLUTION
32	VI. CALIBRATION AT THE ROENTGEN KILOVOLTAGE GENERATOR
32	VII. DISCUSSION OF EXPERIMENTAL RESULTS
32	ENERGY CALIBRATION
40	FLUORESCENCE RINGS
42	HIGH-ENERGY RINGS
43	VIII. SUMMARY
48	APPENDIX I. CALIBRATION OF DIFFERENTIAL ENERGY LOSS DISTRIBUTION FOR SCINTILLATION NO. 3 AT 17.6 MeV INCIDENT X-RAY ENERGY
51	Bibliography

LIST OF ILLUSTRATIONS

	Page Number
Figure 1. Physical Arrangement of the Spectrometer	7
Figure 2. Arrangement and Shapes of the Plastic Scintillators	8
Figure 3. Construction of Scintillation Unit No. 1	9
Figure 4. Block Diagram of Experimental Equipment	12
Figure 5. Cable Curve	13
Figure 6. Block Diagram of the Addition and Gating Circuit	14
Figure 7. Block Diagram of the Pulse-Height Analysis Circuit	16
Figure 8. Method of Recording Scaler Lights	17
Figure 9. Calculated Differential Energy Distribution Curves for Scintillator No. 2, 17.6 Mev, 16-mil Pb Converter	20
Figure 10. Electron Energy Loss by Radiation	27
Figure 11. The Spectrometer in Place at the M.I.T. Rockefeller Generator	33
Figure 12. Calibration Curve	37
Figure 13. Energy Calibration	39
Figure 14. Pulse Height Distribution for Scintillator No. 2 at 6 Mev	41
Figure 15. Effect of Changing Discriminator No. 1	42
Figure 16. Effect of Changing Discriminator No. 2	44
Figure 17. Effect of the Anticoincidence Circuit at 17 Mev	46

LIST OF ILLUSTRATIONS

Page Number

1	Figure 1. Physical Arrangement of the Spectrometer
2	Figure 2. Arrangement and Shape of the Plastic Scintillator
3	Figure 3. Construction of Scintillation Unit No. 1
12	Figure 4. Block Diagram of Experimental Equipment
13	Figure 5. Cable Curve
14	Figure 6. Block Diagram of the Addition and Gating Circuit
15	Figure 7. Block Diagram of the Pulse-Height Analysis Circuit
17	Figure 8. Method of Recording Scaler Lights
20	Figure 9. Calculated Differential Energy Distribution Curves for Scintillator No. 2, 17.6 Mev, 10-MV Converter
27	Figure 10. Electron Energy Loss by Radiation
32	Figure 11. The Spectrometer in Place at the W.I.T. Rochester Generator
37	Figure 12. Oscillation Curve
39	Figure 13. Energy Calibration
41	Figure 14. Pulse Height Distribution for Scintillator No. 2 at 6 Mev
42	Figure 15. Effect of Changing Discriminator No. 1
44	Figure 16. Effect of Changing Discriminator No. 2
46	Figure 17. Effect of the Antiscatter Circuit at 17 Mev

ACKNOWLEDGMENTS

The author* expresses his appreciation to all those who have helped to make this work possible. He is particularly indebted to Dr. P. T. Demos for friendly guidance and helpful advice throughout the course of this and other work; to Dr. C. P. Sargent for active participation in all phases of the experimental work; to Professor R. D. Evans and Professor B. T. Feld for advice in various phases of the experiment and theory; to Dr. Hans Mark for making the facilities of the Rockefeller generator available and for many other kindnesses and helpful suggestions; to Mr. H. W. Greene for help in the construction of the electronic components.

For the typing and proofreading, the author would like to express his special thanks to Mrs. Mary E. White. Thanks are also due Mrs. Grace Rowe for making the drawings and to Mr. N. Saia for making the block diagrams.

* Enrolled at the Massachusetts Institute of Technology under the United States Naval Postgraduate School system through the sponsorship of the Bureau of Ordnance, Navy Department.

ACKNOWLEDGMENTS

The author^{*} expresses his appreciation to all those who have helped to make this work possible. He is particularly indebted to Dr. P. T. Dumas for friendly guidance and helpful advice throughout the course of this and other work; to Dr. C. P. Sargent for active participation in all phases of the experimental work; to Professor R. D. Evans and Professor B. T. Field for advice in various phases of the experiment and theory; to Dr. Hans Mark for making the facilities of the Rockefeller generator available and for many other kindnesses and helpful suggestions; to Mr. H. W. Green for help in the construction of the electronic components.

For the typing and proofreading, the author would like to express his special thanks to Mrs. Mary E. White. Thanks are also due Mrs. Grace Howe for making the drawings and to Mr. W. Sain for making the block diagrams.

^{*}Enrolled at the Massachusetts Institute of Technology under the United States Naval Postgraduate School system through the sponsorship of the Bureau of Ordnance, Navy Department.

I. INTRODUCTION

The intention of this paper is to describe an x-ray spectrometer designed for use at the M. I. T. linear accelerator. The spectrometer is a three-counter telescope with a thin lead radiator between the first and second counter. The first and second counters are thin plastic scintillators; the third, a thick plastic scintillator. An acceptable event is one in which there is no pulse in the first counter and a doubly ionizing pulse in the second counter in coincidence with the third counter. Such events should be electron-positron pairs originating only in the radiator. To a first approximation, the sum of the pulse heights produced in the second and third counter is proportional to the incident x-ray energy. This chapter is devoted to explaining the need for a spectrometer of this type at the linear accelerator.

Five- to 25-Mev x-rays are known to interact strongly with nuclei. Among the heavier elements, as much as 2 percent of the total absorption coefficient for 25-Mev bremsstrahlung is of nuclear rather than atomic origin. Most of the experiments have investigated the emission of heavy particles following photon absorption. Recently, however, some measurements have been made of nuclear absorption coefficients in good geometry transmission experiments¹ and of large-angle scattering of bremsstrahlung².

X. INTRODUCTION

The intention of this paper is to describe an x-ray spectrometer designed for use at the M. I. T. linear accelerator. The spectrometer is a three-counter telescope with a thin lead radiator between the first and second counter. The first and second counters are thin plastic scintillators; the third, a thick plastic scintillator. An acceptable event is one in which there is no pulse in the first counter and a doubly ionizing pulse in the second counter in coincidence with the third counter. Such events should be electron-positron pairs originating only in the radiator. To a first approximation, the sum of the pulse heights produced in the second and third counter is proportional to the incident x-ray energy. This chapter is devoted to explaining the need for a spectrometer of this type at the linear accelerator.

Five to 35-Mev x-rays are known to interact strongly with matter. Among the heavier elements, as much as 5 percent of the total absorption coefficient for 35-Mev bremsstrahlung is of nuclear rather than atomic origin. Most of the experiments have investigated the excitation of heavy nuclei as follows: following photon absorption. Recently, however, some measurements have been made of nuclear absorption coefficients in good geometry transmission experiments and of large-angle scattering of bremsstrahlung.^{1,2}

The M. I. T. linear accelerator is 10 to 100 times as strong a source of 5- to 17-Mev x-rays as the usual betatron of comparable energy. This accelerator can furnish average electron currents of about 2 microamperes. It is, however, a pulsed machine with a duty ratio of only 10^{-4} , and during the 1 microsecond pulse, the current reaches peaks of about 50 milliamperes. The low-duty ratio of the accelerator is a very important factor in the design of an x-ray spectrometer for use at the M.I.T. linear accelerator. The counting rate of a detector can be no more than a few counts per second, and the detector must be able to operate in the presence of a very high level of background radiation (low-energy photons and fast neutrons) present during the 1 microsecond pulse. One must use this high photon intensity of the accelerator to obtain energy resolution, good geometry, or small target size, rather than to obtain high counting rates.

A second limitation of the M. I. T. linear accelerator as a photon source imposes further restrictions on a photon detector. The electron energy spectrum of the accelerator is not only far from monochromatic, but it is difficult to keep the spectrum constant during a run and difficult to reproduce the same spectrum on subsequent runs. If one is to use all the current available and, say, thick-target bremsstrahlung in order to make as strong a photon source as possible, it is:

1. Necessary to monitor the photon spectrum itself rather than the electron current; and

The M. I. T. linear accelerator is 10 to 100 times as strong a source of 2- to 17-Mev x-rays as the usual betatron of comparable energy. This accelerator can furnish average electron currents of about 2 microamperes. It is, however, a pulsed machine with a duty ratio of only 10^{-4} , and during the 1 microsecond pulse, the current reaches peaks of about 20 milliamperes. The low-duty ratio of the accelerator is a very important factor in the design of an x-ray spectrometer for use at the M. I. T. linear accelerator. The counting rate of a detector can be no more than a few counts per second, and the detector must be able to operate in the presence of a very high level of background radiation (low-energy photons and fast neutrons) present during the 1 microsecond pulse. One must use this high photon intensity of the accelerator to obtain energy resolution, good geometry, or small target size, rather than to obtain high counting rates. A second limitation of the M. I. T. linear accelerator as a photon source imposes further restrictions on a photon detector. The electron energy spectrum of the accelerator is not only far from monoenergetic, but it is difficult to keep the spectrum constant during a run and difficult to reproduce the same spectrum on subsequent runs. It is to use all the current available and, say, thick-target bremsstrahlung in order to make as strong a photon source as possible, it is necessary to monitor the photon spectrum itself rather than the electron current; and

2. Very desirable to obtain as much information as possible from a single run.

The most efficient photon detector with reasonable resolution is a large volume of NaI. Such a spectrometer has been constructed by Koch³. Koch's best detector is a total absorption spectrometer with 11 percent resolution at 11 Mev, employing a NaI crystal 5 x 8 inches. His 2 x 2 x 5-inch NaI crystal gives about 20 percent resolution at 10 Mev. For use at the accelerator, the expense of such a large amount of NaI would perhaps be justified were it not for

1. The extreme sensitivity of NaI to photon radiation;
2. Its relative slow decay time of about 0.3 μ sec.

The first limitation requires the spectrometer to be enclosed in a massive amount of shielding. In a large-angle photon scattering experiment, the signal would need to be clipped to a fraction of the decay time of NaI to reduce pile-up of Compton recoil electrons. The differential cross section for Compton scattering at 90 degrees is as much as 10^5 times as large as cross sections one would like to measure, and the pile-up of the approximately half Mev Compton scattered photons during the 1 μ second accelerator pulse is a serious problem with any photon detector which involves pulse-height analysis.

The best energy resolution in the 5- to 17-Mev region is obtained with a magnetic pair spectrometer. Walker and McDaniel⁴ were among the first in this field and obtained a solid angle times efficiency of approximately 10^{-7} with an energy resolution (width at half

5. Very desirable to obtain as much information as pos-

sible from a single run.

The most efficient photon detector with reasonable resolution

is a large volume of NaI. Such a spectrometer has been constructed

by Kosh. Kosh's best detector is a total absorption spectrometer

with 11 percent resolution at 11 Mev, employing a NaI crystal 2×8

inches. His $2 \times 2 \times 2$ -inch NaI crystal gives about 20 percent resolu-

tion at 10 Mev. For use at the accelerator, the expense of such a

large amount of NaI would perhaps be justified were it not for

1. The extreme sensitivity of NaI to photon radiation;

2. Its relative slow decay time of about 0.3μ sec.

The first limitation requires the spectrometer to be enclosed

in a massive amount of shielding. In a large-angle photon scattering

experiment, the signal would need to be clipped to a fraction of the

decay time of NaI to reduce pile-up of Compton recoil electrons. The

differential cross section for Compton scattering at 90 degrees is as

much as 10^2 times as large as cross sections one would like to measure,

and the pile-up of the approximately half Mev Compton scattered photons

during the 1μ second accelerator pulse is a serious problem with any

photon detector which involves pulse-height analysis.

The best energy resolution in the 2- to 15-Mev region is ob-

tained with a magnetic belt spectrometer. Walker and McDaniel¹⁴ were

among the first in this field and obtained a solid angle three times effi-

ciency of approximately 10^{-5} with an energy resolution (width at half

maximum) of 5.5 percent. Currently, the best energy resolution in the 5- to 17-Mev energy range is obtained by Kinsey and Bartholomew⁵, using a similar improved version of Walker and McDaniel's magnetic pair spectrometer. Using a 4.7 milligram/cm² gold radiator, Kinsey's best half-width is 140 kev, independent of photon energy.

The linear accelerator is a sufficiently strong source of x-rays to enable one to utilize a high-resolution, low-efficiency magnetic pair spectrometer. It should be able to measure the entire energy spectrum at one time; hence, it would have many channels and be of large size.

Another type of spectrometer, known as the three-crystal scintillation spectrometer⁶⁻⁸, employing three NaI 1-1/2 inch diameter crystals proves useful in the 4- to 12-Mev energy range. A typical arrangement⁶ employs two 1-1/2 inch by 1 inch thick NaI crystals as annihilation radiation detectors and a center 1-1/2 inch by 4 inch long NaI crystal which measures the energy of the coincidence pair. Counter efficiency at 6 Mev is about 10^{-5} , and width at half maximum is 7 percent.

Energy resolution with this three-crystal scintillation spectrometer at 11 Mev is 11 percent. In addition to those limitations imposed by the linear accelerator on the NaI total absorption spectrometer, the three-crystal scintillation spectrometer depends on 0.51-Mev photons in coincidence for its resolution, and hence is not easily adaptable for use at the M.I.T. linear accelerator.

maximum) of 2.5 percent. Currently, the best energy resolution in the 7- to 17-Mev energy range is obtained by Kinsey and Bartholomew, using a similar improved version of Walker and McDaniel's magnetic pair spectrometer. Using a 0.7 milligram/cm² gold radiator, Kinsey's best half-width is 110 kev, independent of photon energy.

The linear accelerator is a sufficiently strong source of x-rays to enable one to utilize a high-resolution, low-efficiency magnetic pair spectrometer. It should be able to measure the entire energy spectrum at one time; hence, it would have many channels and be of large size.

Another type of spectrometer, known as the three-crystal coincidence spectrometer, employing three NaI 1-1/2 inch diameter crystals proves useful in the 4- to 12-Mev energy range. A typical arrangement employs two 1-1/2 inch by 1 inch thick NaI crystals as annihilation radiation detectors and a center 1-1/2 inch by 4 inch long NaI crystal which measures the energy of the coincidence pair. Counter efficiency at 6 Mev is about 10%, and width at half maximum is 7 percent.

Energy resolution with this three-crystal coincidence spectrometer at 11 Mev is 11 percent. In addition to these limitations imposed by the linear accelerator on the NaI total absorption spectrometer, the three-crystal coincidence spectrometer depends on 0.51-Mev photons in coincidence for its resolution, and hence is not easily adaptable for use at the M.I.T. linear accelerator.

A fourth approach to the problem has been attempted, which should provide:

1. Approximately 10 percent resolution at 10 Mev;
2. Small dimensions and ease of shielding;
3. Solid-angle times efficiency of about 10^{-4} ;
4. Ability to measure an entire spectrum of photons from 5- to 17-Mev at a single run with several bins per resolution width;
5. Simplicity and economy as far as the actual detection is concerned. The major investment would go into the design and construction of associated electronic equipment. This same equipment would be useful for other projects at the M. I. T. accelerator (see, for example, W. J. Sawtelle, S.M. Thesis, M.I.T., May 1955).

A fourth approach to the problem has been attempted, which

should provide:

1. Approximately 10 percent resolution at 10 MeV;

2. Small dimensions and ease of shielding;

3. Solid-angle times efficiency of about 10^{-4} ;

4. Ability to measure an entire spectrum of photons

from 2- to 17-MeV at a single run with several times per resolution

width.

2. Simplicity and economy as far as the actual detector

is concerned. The major investment would go into the design and

construction of associated electronic equipment. This same equipment

would be useful for other projects at the W. I. T. Accelerator (see,

for example, W. J. Swank, R. W. Thoma, W. I. T., May 1952).

II. APPARATUS

DESCRIPTION OF SPECTROMETER

The spectrometer scintillators are commercially available "Pilot B" crystals, density 1.03, polyvinyl toluene, para-terphenyl, para-para-prime diphenylstilbene¹⁹. Preliminary measurements indicate a decay time of less than 3×10^{-9} seconds²⁰. Figure 1 shows to scale the physical arrangement of the spectrometer. The beam of photons from the source being surveyed is collimated by means of a half-inch hole in a 3-inch thick lead disk. The collimated photons are then incident on a lead foil where they interact forming pairs and Compton recoil electrons. This foil is known as the "converter." The converter is one-half inch in diameter, cemented to a thin lucite ring. The converter fits flush against scintillator No. 2, which in turn is held flush against scintillator No. 1. No. 2 scintillator is a cylinder $3/4$ inch in diameter by $3/16$ inch thick; No. 1 scintillator is a tapered cylinder 3 inches long, tapering from $2-1/4$ inches in diameter to $1-1/2$ inches in diameter one-half inch from the end. Figure 2 shows the shape and arrangement of the plastic scintillators.

Scintillator No. 1 has all its open faces wrapped in 1-mil aluminum foil to improve the light collection and to separate optically scintillator No. 1 from scintillator No. 2. The scintillation unit comprises the plastic scintillator, optical coupling, and selected RCA 5819 phototube. Figure 3 shows to scale the method of construction of unit No. 1.

II. APPARATUS

DESCRIPTION OF SPECTROMETER

The spectrometer scintillators are commercially available "Pilot 8" crystals, density 1.03, polyvinyl toluene, para-terphenyl, para-phenylene diisocyanate¹². Preliminary measurements indicate a decay time of less than 3×10^{-8} seconds. Figure 1 shows the scale of the physical arrangement of the spectrometer. The beam of photons from the source being surveyed is collimated by means of a half-inch hole in a 3-inch thick lead disk. The collimated photons are then incident on a lead foil where they interact forming pairs and Compton recoil electrons. This foil is known as the "converter." The converter is one-half inch in diameter, cemented to a thin Lucite ring. The converter lies flush against scintillator No. 2, which in turn is held flush against scintillator No. 1. No. 2 scintillator is a cylinder $3\frac{1}{2}$ inch in diameter by $3\frac{1}{2}$ inch thick; No. 1 scintillator is a tapered cylinder 3 inches long, tapering from $2\frac{1}{2}$ inches in diameter to $1\frac{1}{2}$ inches in diameter one-half inch from the end. Figure 2 shows the shape and arrangement of the plastic scintillators. Scintillator No. 1 has all its open faces wrapped in 1-mil aluminum foil to improve the light collection and to separate optically scintillator No. 1 from scintillator No. 2. The scintillation unit comprises the plastic scintillator, optical coupling, and selected RCA 6819 phototubes. Figure 3 shows the method of construction of unit No. 1.

Figure 1

Physical Arrangement of the Spectrometer

The axis of scintillator unit No. 3 is perpendicular to both the axis of unit No. 2 and unit No. 1.

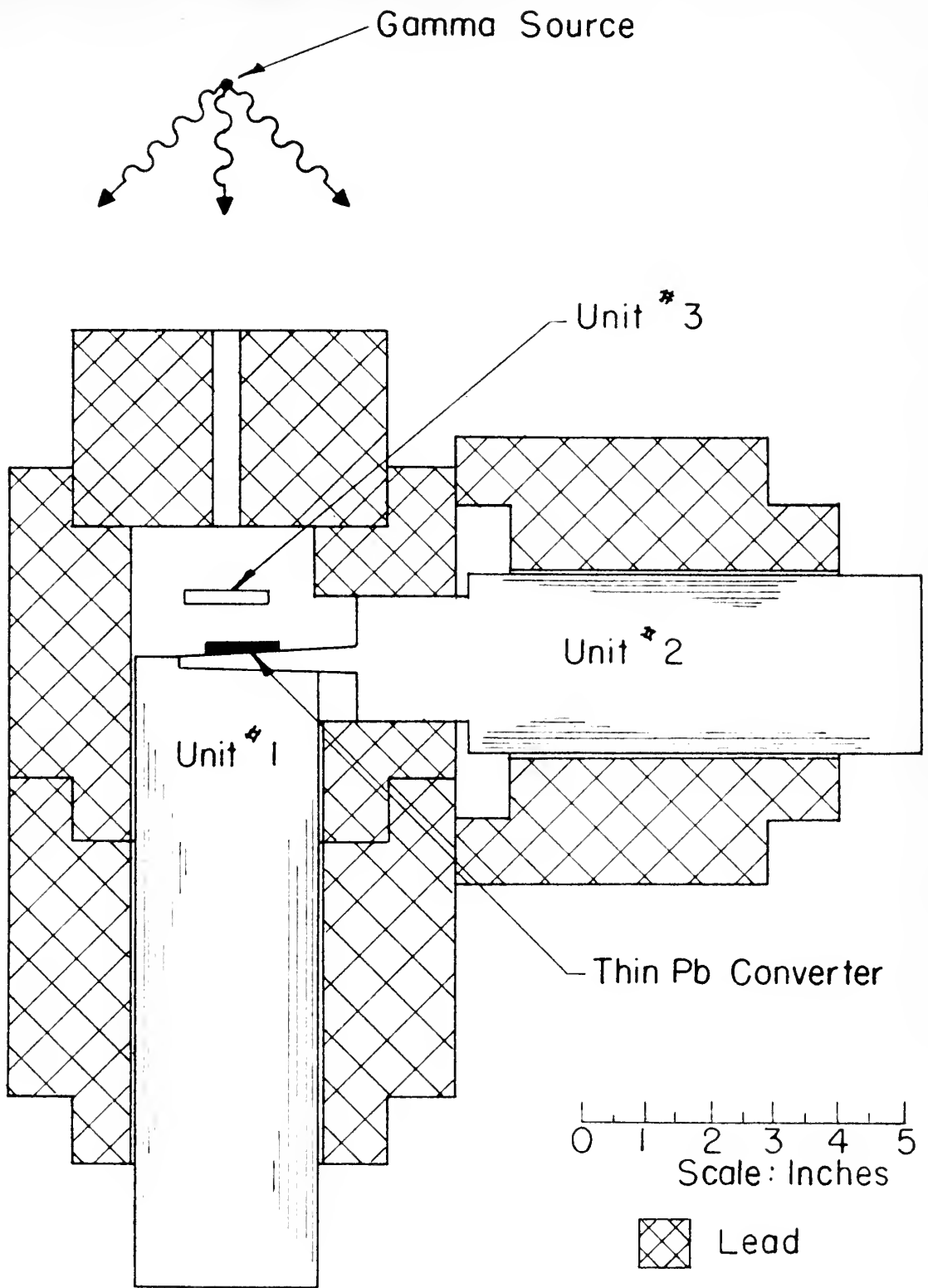
Figure 1

Physical arrangement of the spectrometer

The axis of rotation unit No. 3 is

perpendicular to both the axis of unit

No. 2 and unit No. 1.



SHIELDING ARRANGEMENT

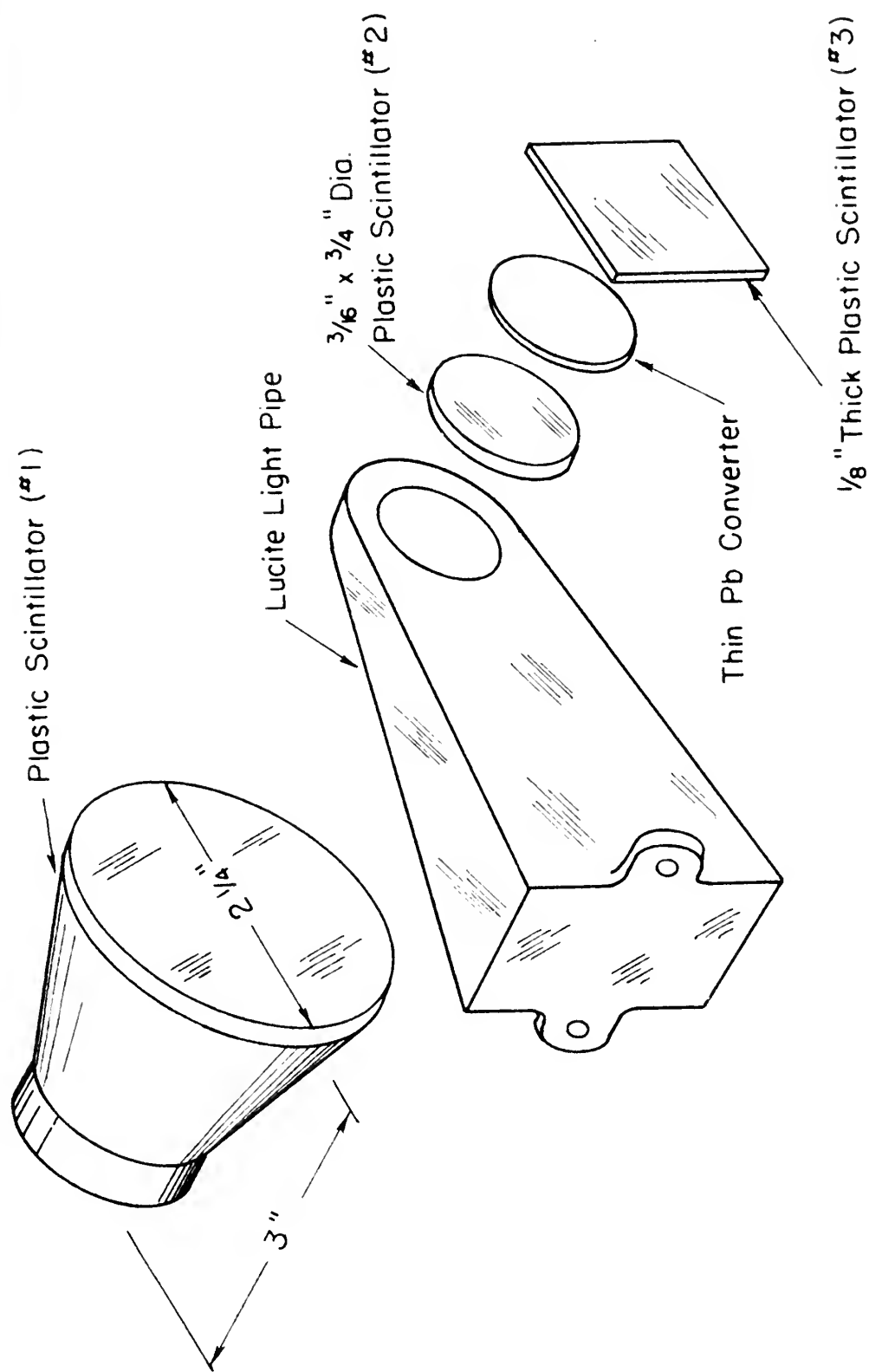
Figure 2

Arrangement and Shapes of the
Plastic Scintillators

Plastic scintillator No. 2 is a push fit into
the lucite light pipe. The converter, No. 2
scintillator, and scintillator No. 1 are held
together by a clamp arrangement.

Figure 2
Arrangement and Shapes of the
Plastic Scintillators

Plastic scintillator No. 2 is a push fit into the lucite light pipe. The converter, No. 2 scintillator, and scintillator No. 1 are held together by a clamp arrangement.



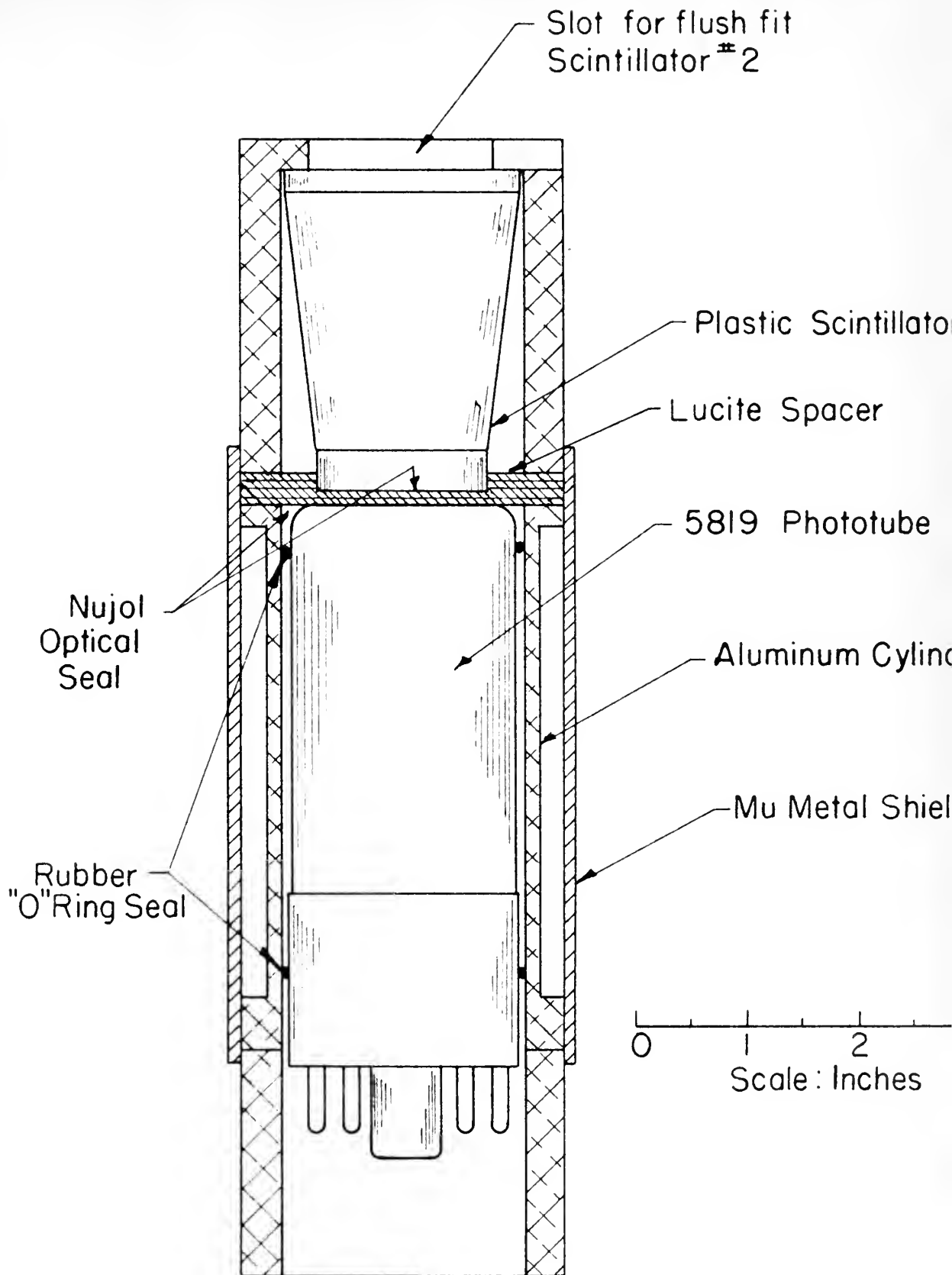
ARRANGEMENT OF PLASTIC SCINTILLATORS

Figure 3

Construction of Scintillation Unit No. 1.

Figure 3

Construction of Reinforcement Unit No. 1



SCINTILLATION UNIT #1

Scintillator unit No. 2 has a 1-1/2 inch diameter, 2 inch long lucite light pipe, to which is screwed the 2-1/2 inch lucite light pipe shown in Figure 2. Scintillator No. 2 is inserted in the light pipe (push fit, Mjøl optical seal). The converter holder fits into a larger diameter, 1/4 inch thick lucite ring which clamps unit No. 1 and unit No. 2 together.

Scintillator No. 3 is 1/8 inch by 1-1/8 inch, rectangular cross section, 2 inches long (shown in Figure 2). This domino-shaped plastic scintillator is held by a lucite clamp so that the standard 1-1/2 inch diameter lucite light pipe (as described for scintillator No. 2) looks at it end on.

ELECTRONIC CIRCUIT

The experimental equipment is shown in the block diagram of Figure 4. The gain of the system is calibrated by introducing artificial pulses (employing a Western Electric 275B relay to develop pulses of proper shape) into the input of the preamplifier. The height of these pulses is measured to an accuracy of a few tenths of a percent. The preamplifier is physically located as an integral part of the scintillation unit, bolted to the end of the aluminum housing of Figure 3. Pulses are then amplified times 30 in an amplifier whose rise time is 0.04 μ second. Unit No. 1 and unit No. 2 have two outputs. One output goes to the coincidence circuit and

Scintillator unit No. 2 has a $1-1/2$ inch diameter, 2 inch long
inside light pipe, to which is screwed the $2-1/2$ inch inside light
pipe shown in Figure 2. Scintillator No. 2 is inserted in the light
pipe (push fit, metal optical seal). The converter holder fits into
a larger diameter, $1/4$ inch thick inside ring which clamps unit No. 1
and unit No. 2 together.

Scintillator No. 3 is $1/8$ inch by $1-1/8$ inch, rectangular cross
section, 2 inches long (shown in Figure 2). This domino-shaped piece
the scintillator is held by a inside clamp so that the standard $1-1/2$
inch diameter inside light pipe (as described for scintillator No. 2)
locks at its end on.

KINETIC CIRCUIT

The experimental equipment is shown in the block diagram of
Figure 1. The gain of the system is calibrated by introducing arti-
ficial pulses (employing a Western Electric 275 relay to develop
pulses of proper shape) into the input of the preamplifier. The
height of these pulses is measured to an accuracy of a few tenths of
a percent. The preamplifier is physically located as an integral
part of the scintillation unit, bolted to the end of the aluminum
housing of Figure 3. Pulses are then amplified times 30 in an ampli-
fier whose rise time is 0.04 μ second. Unit No. 1 and unit No. 2
have two outputs. One output goes to the coincidence circuit and

the other to the addition circuit. The coincidence outputs from unit No. 1 and unit No. 2 are delay-line clipped to 0.05μ second and delayed by 0.03μ second to allow time for anticoincidence pulse No. 3 to function. These pulses are amplified and fed into an EFP 60-pulse shaper. The function of D2 is to discriminate against the Compton recoil electrons. D1 allows the biasing out of low-energy photons if desired. The output of EFP 60 No. 3 goes to the grid of the No. 2 Philips tube. Since the two inputs of the No. 2 EFP 60 are out of phase, if a signal exists at No. 3, there is no output from No. 2. The outputs of the No. 1 and No. 2 pulse shapers go to a diode bridge.

The measurement of the resolving time of the spectrometer was experimentally determined, using the 6-Mev fluorine gamma-ray, to be 0.057μ second, as shown in Figure 5. A DuMont 6292 phototube was tried in unit No. 1 but proved to be unsatisfactory. The fluctuations in the transit time for the DuMont tube were so large that the cable curve was not flat on top.

The other outputs from the No. 1 and No. 2 (x 30) amplifiers are added, clipped to 0.08μ second, stretched, and amplified as shown by the block diagram of Figure 6. The output from the diode-bridge coincidence circuit triggers a univibrator which forms a 10μ second gate. If the gate is open, the added pulse gets through and is amplified and then is pulse height analyzed.

the other to the addition circuit. The coincidence outputs from unit No. 1 and unit No. 2 are delay-line aligned to 0.02 μ second and delayed by 0.03 μ second to allow time for anticoincidence pulse No. 3 to function. These pulses are amplified and fed into an RFP 60-mesh trigger. The function of 03 is to discriminate against the counter record spectrum. It allows the passing out of low-energy photons if desired. The output of RFP 60 No. 3 goes to the grid of the No. 3 Miller tube. Since the two inputs of the No. 3 RFP 60 are out of phase, if a signal exists at No. 3, there is no output from No. 3. The outputs of the No. 1 and No. 2 pulse shapers go to a diode bridge.

The measurement of the resolving time of the spectrometer was experimentally determined, using the 6-Mev fluorine gamma-ray, to be 0.027 μ second, as shown in Figure 5. A DuMont 6395 phototube was tried in unit No. 1 but proved to be unsatisfactory. The fluctuations in the signal time for the DuMont tube were so large that the pulse curve was not flat on top.

The other outputs from the No. 1 and No. 2 (x 30) amplifiers are added, aligned to 0.02 μ second, stretched, and amplified as shown by the block diagram of Figure 6. The output from the diode bridge coincidence circuit triggers a multivibrator which forms a 10 μ second gate. If the gate is open, the added pulse gets through and is amplified and then its pulse height measured.

Figure 4

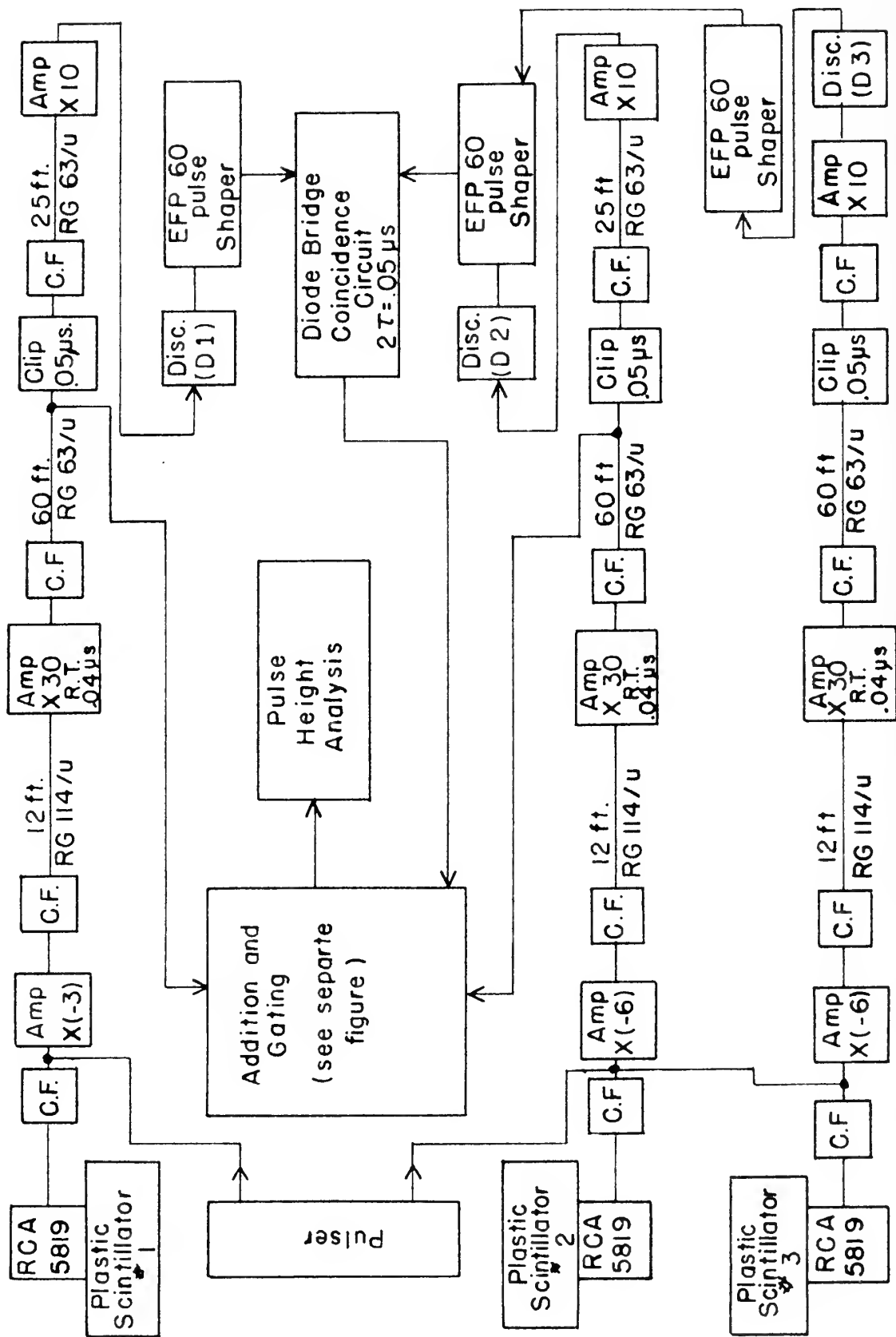
Block Diagram of Experimental Equipment

The addition and gating circuit is shown in Figure 6, the pulse-height analysis circuit in Figure 7.

Figure 1

Block Diagram of Experimental Equipment

The addition and gating circuit is shown in
Figure 6, the pulse-width analyzer circuit
in Figure 7.



BLOCK DIAGRAM OF EXPERIMENTAL EQUIPMENT

Figure 5

Cable Curve

RG 63/U was used in conjunction with a $F^{19}(p, \alpha' \gamma)$ source to determine experimentally the resolving time of the spectrometer. Each run was normalized to the same number of protons incident on the proton target.

Figure 2

Alpha Curve

As α/β was used in conjunction with a
Fig. 2, α/β source to determine experimen-
tally the resolving time of the spec-
trum. Each run was normalized to the
same number of protons incident on the
proton target.

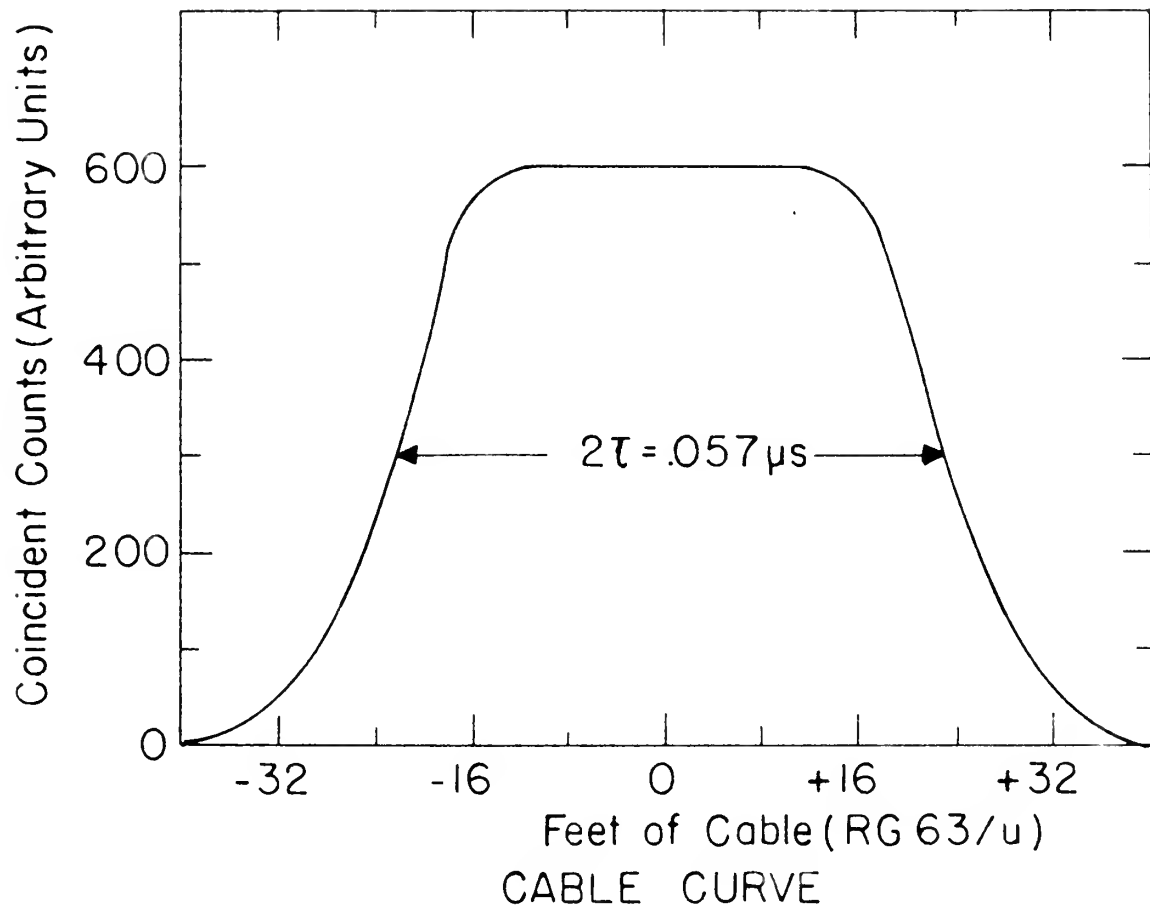
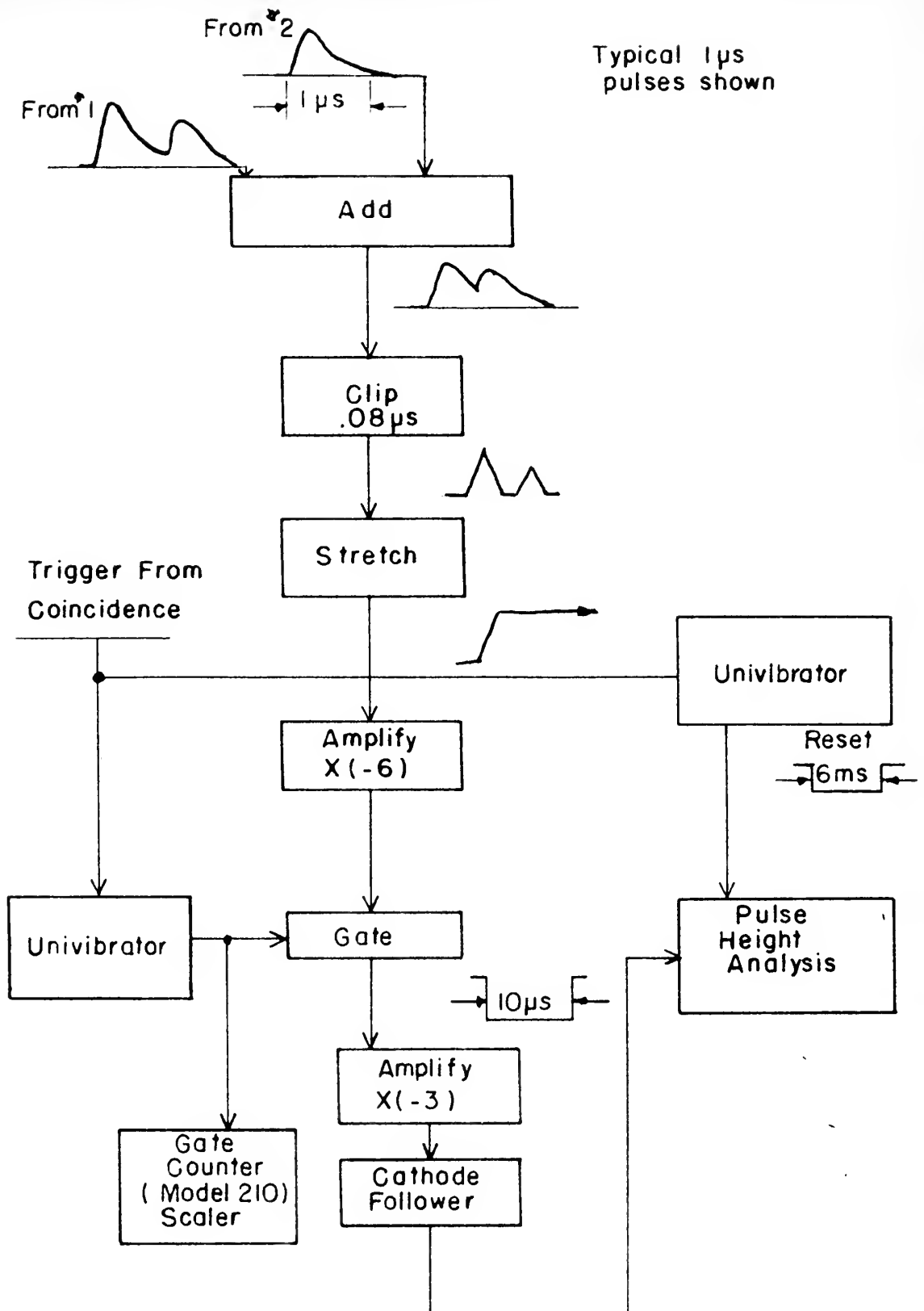


Figure 6

Block Diagram of the Addition and Gating Circuit.

Figure 6

Block Diagram of the Addition and Carrying Circuit.



ADDITION AND GATING CIRCUIT

The pulse-height analysis circuit-block diagram is given in Figure 7. The basic principle of this pulse-height analysis is that pulse height is changed to time by a condenser discharging at constant current through a pentode. This time is accurately measured by beating a crystal-controlled oscillator on the triangular pulse and counting the oscillator pulses by a conventional binary scaler. This circuit is known as the "Multichannel Differential Discriminator," and its detailed circuit diagram may be found on file 6432, Laboratory for Nuclear Science, M. I. T., Dwg. No. D-2231-A. The output of the scaler goes to a buffer amplifier and then to one of two (or both simultaneously) methods of recording the reading of the scaler.

Figure 8 shows one method of data recording. This method provides a 128-channel recording pulse-height analyzer. Six scaler lights are in a light-tight box where they are recorded by a standard 16-mm movie camera externally driven at approximately 9 inches per minute. The framing pawl of the camera is removed to achieve continuous movement of the film. This is necessary, since the film is "framed" even though the camera shutter has been removed and made inoperative. A clock is an added feature for future identification. The film is read most easily by scanning it on a standard 16-mm microfilm reader. The pulser is turned on periodically during a run for calibration purposes. Reading time varies from 150 - 400 counts per hour, depending on energy and counting rate.

The pulse-height analysis circuit-block diagram is given in

Figure 7. The basic principle of this pulse-height analysis is that pulse height is changed to time by a constant discharging of constant current through a pentode. This time is accurately measured by feeding a crystal-controlled oscillator on the triangular pulse and counting the oscillator pulses by a conventional binary scaler. This circuit is known as the "Multichannel Differential Discriminator", and its detailed circuit diagram may be found on file 6132, Laboratory for Nuclear Science, M. I. T., Wg. No. D-2231-A. The output of the scaler goes to a buffer amplifier and then to one of two (or both simultaneously) methods of recording the reading of the scaler.

Figure 8 shows one method of data recording. This method provides a 158-channel recording pulse-height analyzer. Six scaler lights are in a light-tight box where they are recorded by a standard 16-mm movie camera externally driven at approximately 9 inches per minute. The framing pawl of the camera is removed to achieve continuous movement of the film. This is necessary, since the film is "frozen" even though the camera shutter has been removed and made insensitive. A clock is an added feature for future identification. The film is read most easily by scanning it on a standard 16-mm microfilm reader. The pulser is turned on periodically during a run for calibration purposes. Reading time varies from 150 - 400 counts per hour, depending on energy and counting rate.

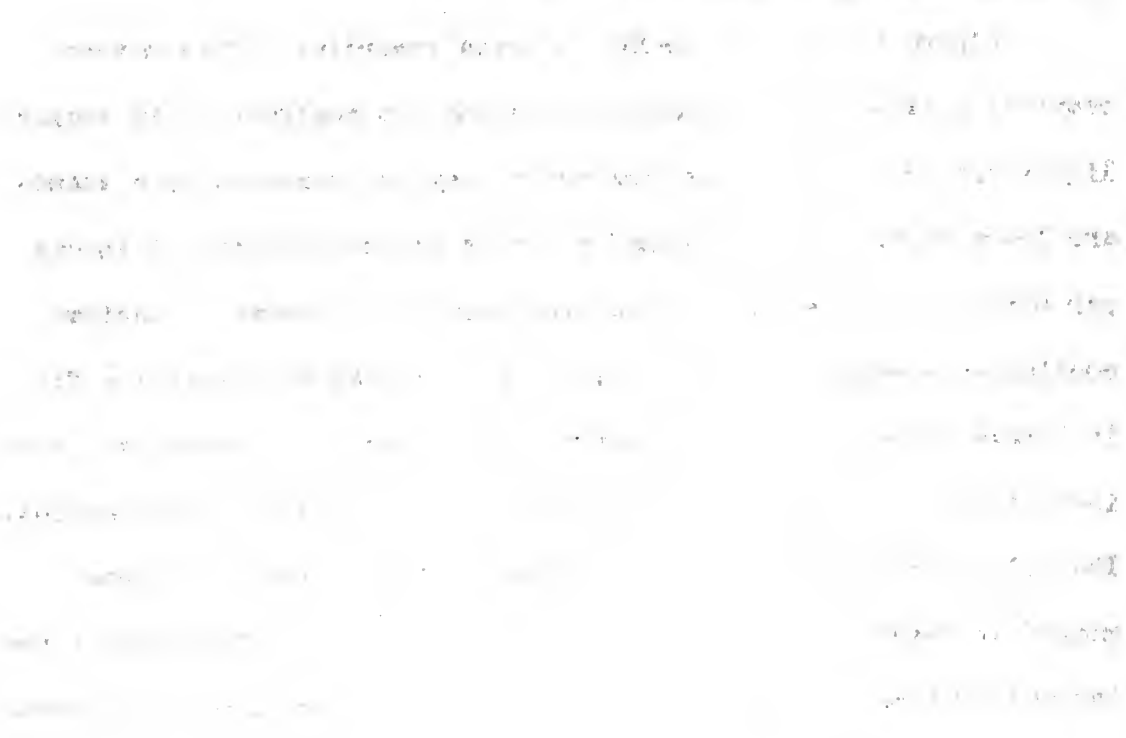
Figure 7

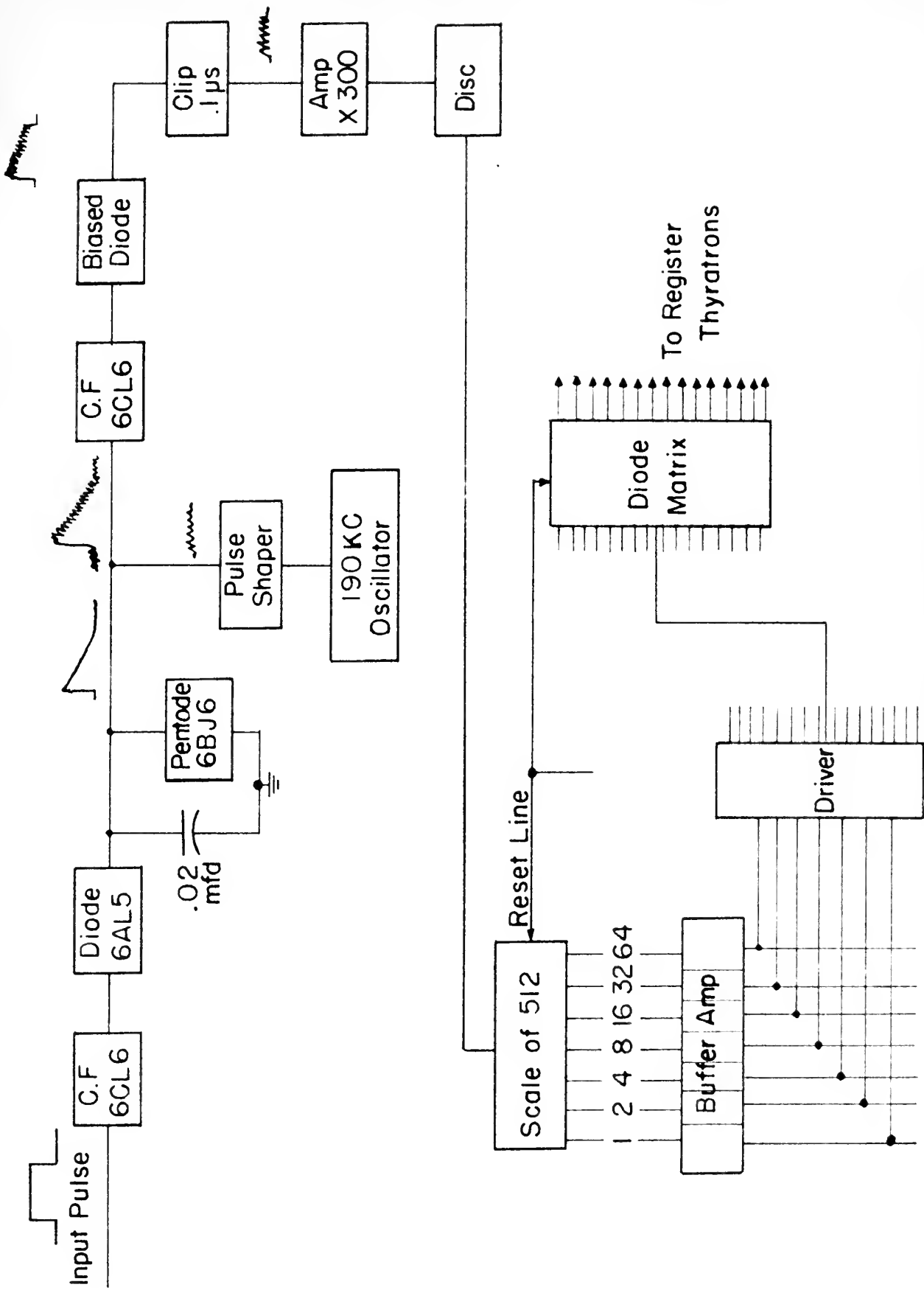
Block Diagram of the Pulse-Height Analysis Circuit



Figure 1

Block Diagram of the Pulse-Height Analysis Circuit





PULSE HEIGHT ANALYSIS CIRCUIT

Figure 8

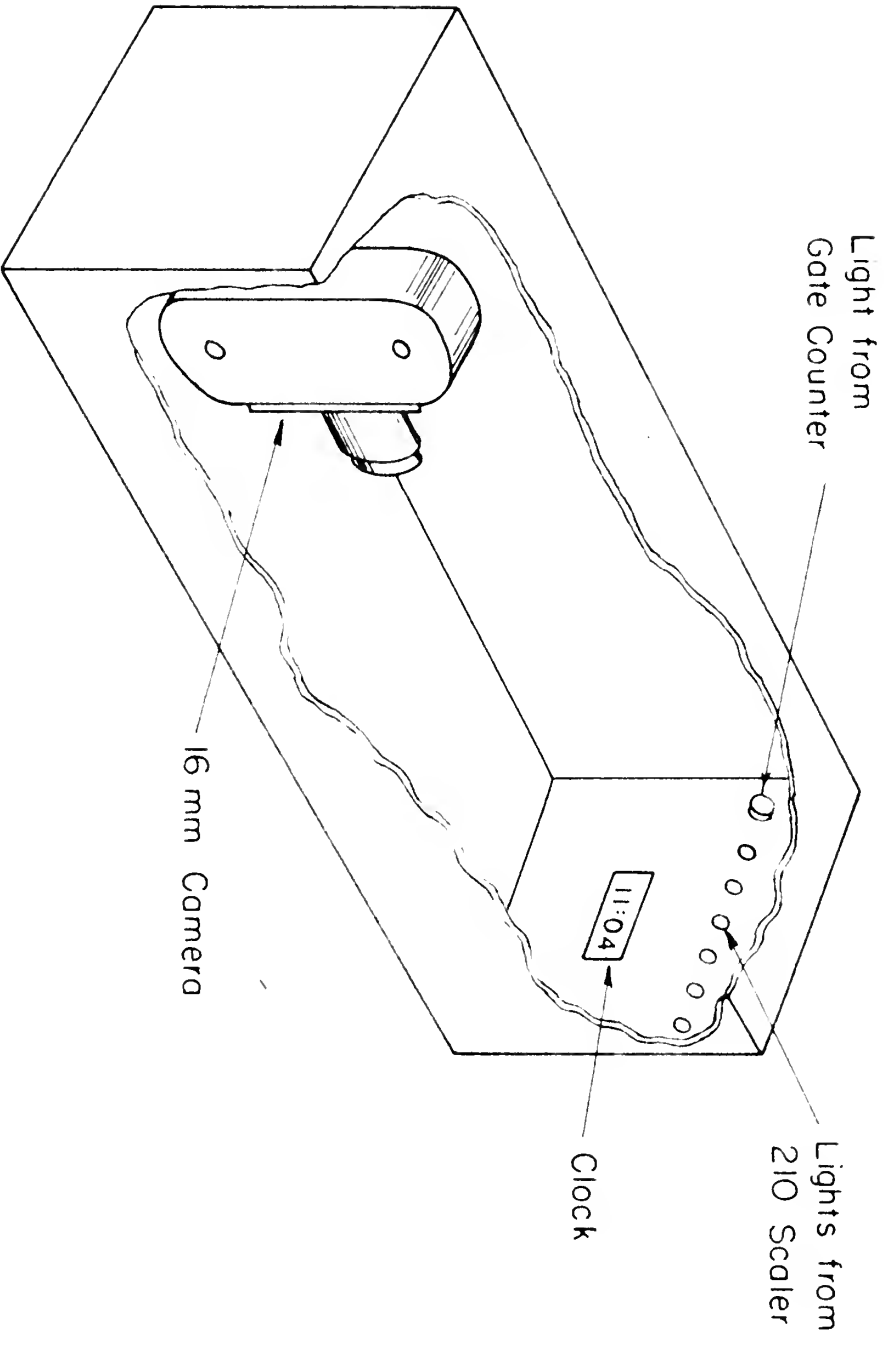
Method of Recording Scaler Lights

The rectangular box shown in the figure is light-tight and a standard 16-mm movie camera, equipped with a short focal length lens, records the fact that the gate was opened and the channel number. The film is externally driven at 9 inches per minute. The clock is for identification of the run.

Figure 8

Method of Recording Radar Lights

The rectangular box shown in the figure is
light-tight and a standard 16-mm movie
camera, equipped with a short focal length
lens, records the fact that the gate was
opened and the channel number. The film is
externally driven at 9 inches per minute.
The clock is for identification of the run.



Light from
Gate Counter

Lights from
210 Scaler

Clock

16 mm Camera

The second method of recording the output of the analyzer is on a set of sixteen mercury registers. Essentially, the binary system of the scaler lights is converted into a scale of sixteen by means of a diode matrix. The sixteen registers can be set (by selector switch) to cover:

- a. Channels 0-15, 16-31, 32-47, ..., 112-127;
- b. Channels 0-31, 32-64, etc; or
- c. Channels 0-63 and 64-127.

Investigation of the overall electronic stability of the spectrometer has shown a drift of the order of 1 percent during a period of one hour. It has been determined that the major part of the drift originates in the addition circuit. The pulse-height analyzer itself is stable to 1 percent over a period of several hours.

The second method of recording the output of the analyzer is on a set of sixteen mercury registers. Essentially, the binary system of the scaler lights is converted into a scale of sixteen by means of a slide matrix. The sixteen registers can be set (by selector switch) to cover:

- a. Channels 0-15, 16-31, 32-47, ... , 112-127;
- b. Channels 0-31, 32-63, etc; or
- c. Channels 0-63 and 64-127.

Investigation of the overall electronic stability of the spectrometer has shown a drift of the order of 1 percent during a period of one hour. It has been determined that the major part of the drift originates in the addition circuit. The pulse-height analyzer itself is stable to 1 percent over a period of several hours.

III. SELECTION OF PAIRS

The principle of selection of pairs created in the converter and rejection of Compton recoil electrons is accomplished by a discriminator in the output of unit No. 2 (D2 of Figure 4). Pairs are mostly emitted in the forward direction with the mean angle of bipartition given to a close approximation²¹ by $\theta_1 = mc^2/E_p$, where $mc^2 = 0.51$ Mev, and E_p = photon energy less 1.02 Mev. The collision energy loss per cm for 1- to 15-Mev electrons is constant within 10 percent if the density effect²³ is included. Hence, to a first approximation, a pair will lose twice as much energy in scintillator No. 2 as will a Compton recoil electron. Therefore, we require that a minimum energy loss be sustained in scintillator No. 2 in order to record a coincidence with scintillator No. 1, resulting in addition of the energy lost by collision in Nos. 1 and 2, and yielding a pulse whose height is linearly proportional to the energy of the incident photon less 1.02 Mev.

For 17-Mev incident x-rays one would expect that D2 would do a good job of separating out the pairs. Figure 9 is an estimate of the pulse-height distribution for the 17.6-Mev incident gamma. Appendix I describes the method of obtaining this figure. One need only set D2 at 1.15-Mev energy loss in order to insure adequate pair selection.

III. PRINCIPLES OF PAIRS

The principle of selection of pairs created in the converter and rejection of Compton recoil electrons is accomplished by a discriminator in the output of unit No. 2 (see Figure 1). Pairs are mostly emitted in the forward direction with the mean angle of distribution given to a close approximation by $\theta_0 = \arccos \sqrt{2}$, where θ_0 is the angle between the direction of motion of the pairs and the direction of the incident photon. The collision energy loss per electron for 1- to 1.5-MeV electrons is constant with an error of 10 percent at the density effect is included. Hence, to a first approximation, a pair will lose twice as much energy in a material as a single electron. Therefore, we require that the minimum energy loss be sustained in scintillator No. 2 in order to record a coincidence with scintillator No. 1, resulting in addition of the energy lost by collision in Nos. 1 and 2, and yielding a pulse whose height is linearly proportional to the energy of the incident photon less 1.02 MeV.

For 1.5-MeV incident x-rays one would expect that No. 2 would do a good job of separating out the pairs. Figure 2 is an estimate of the pulse-height distribution for the 1.5-MeV incident gamma. Figure 3 describes the method of obtaining this figure. One need only set No. 2 at 1.5-MeV energy loss in order to insure adequate pair selection.

Figure 9

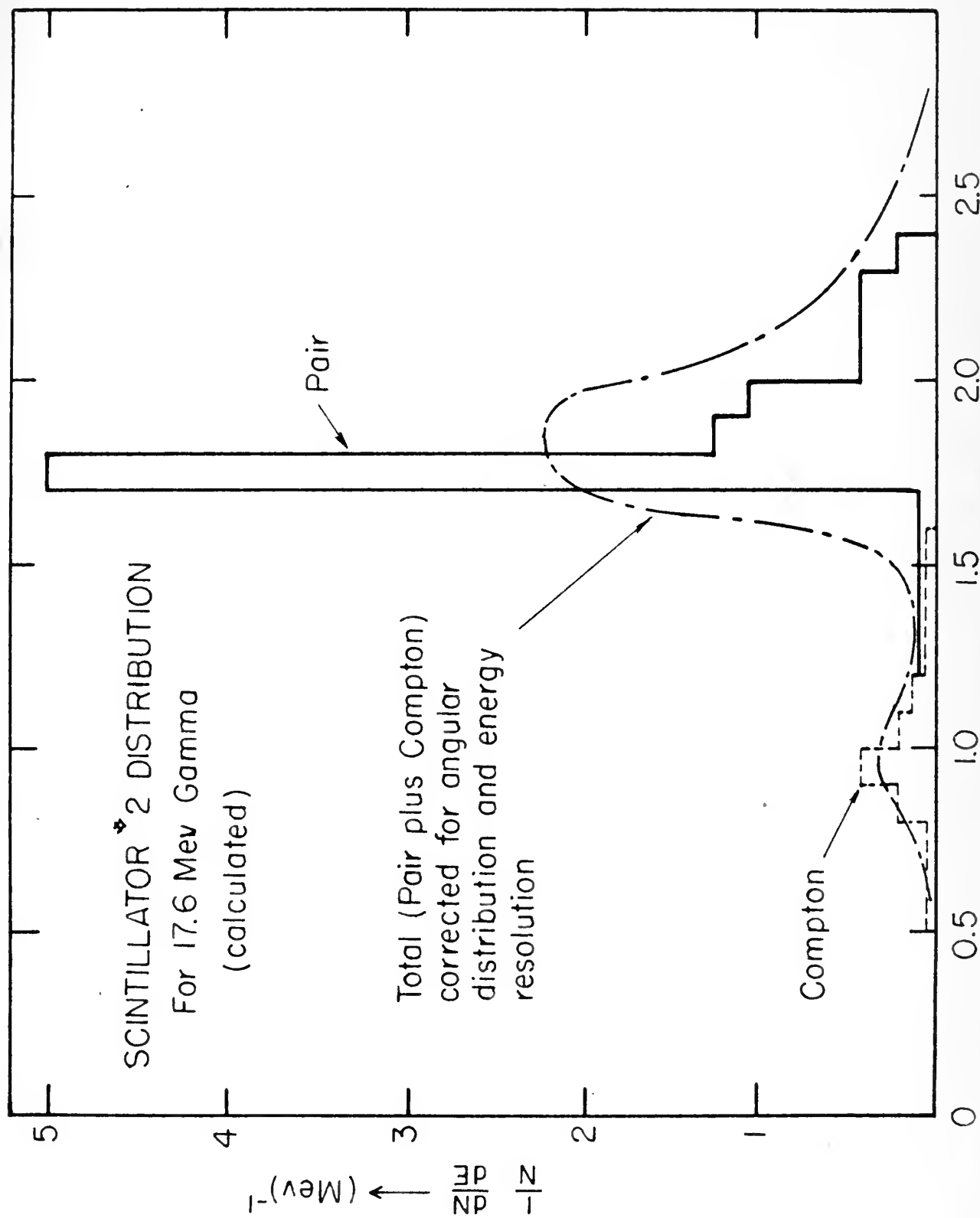
Calculated Differential Energy Distribution Curves
for Scintillator No. 2, 17.6 Mev, 16-mil Pb Converter

The method of calculation of the curves is explained in Appendix I. The contribution to the distribution by pairs and Compton recoil electrons formed in the scintillator itself has not been taken into account.

Figure 2

Calculated Differential Energy Distribution Curves
for Scintillator No. 3, 17.6 MeV, 10-MI 50 Converter

The method of calculation of the curves is ex-
plained in Appendix I. The contribution to
the distribution by noise and Compton recoil
electrons formed in the scintillator itself
has not been taken into account.



At 6 Mev, a worthwhile estimate of the pulse-height distribution for scintillator No. 2 could only be obtained by a detailed "Monte Carlo"¹⁴ calculation, which has not been carried out. It is more difficult to separate the pairs at 6 Mev than at 17 Mev.

Pairs and Compton recoil electrons may originate in scintillators themselves. If these electrons originate in scintillator No. 1, a coincidence will not be recorded. If they originate in the anti-coincidence unit, they will lose enough energy to trigger the anti-coincidence circuit and a coincidence count will not be recorded. However, if these electrons originate in scintillator No. 2, the possibility exists of recording a coincidence count. For comparison purposes, we examine the relative probabilities:

TABLE I

<u>Process</u>	<u>16-mil Lead Converter</u>	<u>Scintillator No. 2</u>	<u>E_{γ}</u>	<u>Reference</u>
Compton	0.7	0.9	6	25
Pair	1.0	0.1	6	44
Compton	0.32	0.39	17	25,29
Pair	2.1	0.25	17	29

Any pairs originating in unit No. 2, which lose enough energy in scintillator No. 2 to trigger D2, will contribute to a sharp resolution function. However, any Compton recoil electrons which are

At 6 Mev, a worthwhile estimate of the pulse-height distribution for scintillator No. 2 could only be obtained by a detailed "Monte Carlo" calculation, which has not been carried out. It is more difficult to separate the pairs at 6 Mev than at 17 Mev. Pairs and Compton recoil electrons may originate in scintillator No. 1. If these electrons originate in scintillator No. 1, a coincidence will not be recorded. If they originate in the anti-coincidence unit, they will lose enough energy to trigger the anti-coincidence circuit and a coincidence count will not be recorded. However, if these electrons originate in scintillator No. 2, the possibility exists of recording a coincidence count. For comparison purposes, we examine the relative probabilities:

TABLE I

Process	Lead Converter	Scintillator No. 2	$\frac{N_2}{N_1}$	Reference
Compton	0.7	0.2	6	25
Pair	1.0	0.1	6	14
Compton	0.32	0.39	17	25, 29
Pair	2.1	0.25	17	29

Any pairs originating in unit No. 2, which lose enough energy in scintillator No. 2 to trigger DS, will contribute to a sharp resolution function. However, any Compton recoil electrons which are

multiply scattered in scintillator No. 2 so as to trigger unit No. 2 (increased path length, increased energy loss by ionization) will result in the broadening of the shape of the spectrum, particularly on the low-energy side, because of the continuous Compton distribution. Qualitatively, it is seen that only low-energy Compton recoil electrons have a large probability of multiple scattering which, combined with their larger angle of emission (Appendix I), make this group the most troublesome. Hence, one way of cutting down the low-energy tail resulting from the Compton effect is to raise the bias of D1 or reduce the thickness of scintillator No. 2.

multiply scattered in scintillator No. 2 so as to trigger unit No. 2
(increased path length, increased energy loss by ionization) will
result in the broadening of the shape of the spectrum, particularly
on the low-energy side, because of the continuous Compton distri-
bution. Qualitatively, it is seen that only low-energy Compton recoils
electrons have a large probability of multiple scattering which,
combined with their larger angle of emission (Appendix I), will this
group the most troublesome. Hence, one way of cutting down the low-
energy tail resulting from the Compton effect is to raise the bias
of D1 or reduce the thickness of scintillator No. 2.

IV. FUNCTION OF SCINTILLATOR NO. 3.

Up to this point, it has been unnecessary to discuss scintillator No. 3 as the operation of the spectrometer as designed only requires unit No. 1 and unit No. 2, as previously described. At the rear surface of scintillator No. 2, there may exist a high-level electron background. Most of these electrons come from the collimator.

For a 17-Mev incident gamma-ray, this large number of scattered electrons is an order of magnitude larger than the number created purposely in the converter. Some of these electrons will lose a sufficient amount of energy in scintillator No. 2 to contribute to the coincidence counting rate.

One can get rid of these electrons either by a magnet or by a third scintillator in anticoincidence. The setting of the discriminator on unit No. 3 is not critical. D3 is set so that a minimum ionizing particle in passing straight through scintillator No. 3 causes the anticoincidence circuit to operate.

IV. FUNCTION OF SCINTILLATOR NO. 3.

Up to this point, it has been unnecessary to discuss scintillators. In the operation of the spectrometer as designed only scintillator No. 1 and No. 2, as previously described. At the same time, it is known that a high-level scintillator No. 3, there may exist a high-level electron background. Most of these electrons come from the collimator. For a 15-degree incident gamma-ray, this large number of scattered electrons is an order of magnitude larger than the number of scattered gamma-rays. Some of these electrons will lose a sufficient amount of energy in scintillator No. 3 to contribute to the coincidence counting rate. One can get rid of these electrons either by a magnet or by a third scintillator in anticoincidence. The setting of the discriminator on unit No. 3 is not critical. It is set so that a minimum ionizing particle in passing straight through scintillator No. 3 causes the anticoincidence circuit to operate.

V. RESOLUTION

Ideally, a monochromatic 5- to 17-Mev x-ray will interact with the converter forming pairs and Compton recoil electrons. As previously discussed, scintillation unit No. 2 will discriminate against the Compton recoil electrons, and pairs only will be recorded as coincidence counts, resulting in a single pulse height corresponding to $E_\gamma - 1.02$, where E_γ is incident monoenergetic x-ray energy in Mev. Resolution is defined as the width in Mev at half maximum divided by the peak energy in Mev.

The resolution of this spectrometer is determined by the following factors:

1. Light collection and photomultiplier statistics;
2. Radiation energy loss in the scintillators;
3. Electron escape from the scintillators;
4. Energy loss in the converter;
5. Capture of one or both annihilation quanta.

LIGHT COLLECTION AND PHOTOMULTIPLIER STATISTICS

The absorption of light is small¹⁷ in plastic scintillators, such as "Pilot B." Photomultiplier statistics can be treated in good approximation^{10,31,32} as a statistical fluctuation in the number of photoelectrons at the first dynode of the photomultiplier.

V. RESOLUTION

Ideally, a monochromatic γ -ray will interact with the converter forming pairs and Compton recoil electrons. As previously discussed, scintillation with No. 5 will discriminate against the Compton recoil electrons, and pairs only will be recorded as coincidence counts, resulting in a single pulse height corresponding to $E_\gamma - 1.02$, where E_γ is incident monochromatic γ -ray energy in Mev. Resolution is defined as the width in Mev at half maximum divided by the peak energy in Mev. The resolution of this spectrometer is determined by the following factors:

1. Light collection and photomultiplier statistics;
2. Radiation energy loss in the scintillator;
3. Electron escape from the scintillator;
4. Energy loss in the converter;
5. Capture of one or both annihilation quanta.

PHOTOMULTIPLIER STATISTICS AND LIGHT COLLECTION

The absorption of light is small ^{if} in plastic scintillators, such as "Pilot B." Photomultiplier statistics can be treated in good approximation ^{10, 11, 12} as a statistical fluctuation in the number of photoelectrons at the first dynode of the photomultiplier.

Mark and Goldring¹³ have measured the resolution of the Cs¹³⁷ 624-kev internal conversion line, using "Pilot B" scintillator and have obtained a value of 15 percent, as compared with 7 percent for NaI. This result implies an average of about 60 photoelectrons per Mev energy loss in the scintillator.

Using this figure of 60 photoelectrons per Mev energy loss and assuming that the light collection efficiency for scintillator No. 2 is half that for scintillator No. 1, we arrive at the following contributions to the energy resolution of the spectrometer resulting from light collection and photomultiplier statistics:

<u>E_γ</u>	<u>Resolution (Percent.)</u>
6	14
10	10
17	7

RADIATION ENERGY LOSS

Electron energy loss by radiation does not contribute to scintillator fluorescence. Bethe and Heitler³⁴ give the probability, P_a , that an electron traversing t radiation lengths will have an energy loss less than a times its initial energy (neglecting loss by ionization) as:

$$P_a = \frac{a^{t/\log 2}}{(t/\log 2)!} ,$$

Mark and Goldring¹³ have measured the resolution of the Cs¹³³

50-kev internal conversion line, using "Pilot B" scintillator and have obtained a value of 12 percent, as compared with 7 percent for NaI. This result implies an average of about 50 photoelectrons per keV energy loss in the scintillator.

Using this figure of 50 photoelectrons per keV energy loss and assuming that the light collection efficiency for scintillator No. 2 is half that for scintillator No. 1, we arrive at the following contributions to the energy resolution of the spectrometer resulting from light collection and photomultiplier statistics:

$\frac{E}{Y}$	Resolution (Percent.)
6	11
10	10
17	7

RADIATION ENERGY LOSS

Electron energy loss by radiation does not contribute to scintillator fluorescence. Bethe and Heitler¹⁴ give the probability, P , that an electron traversing a radiation length will have an energy loss less than a times the initial energy (neglecting loss by ionization) as:

$$P = \frac{e^{\sqrt{2} \log 2}}{(\sqrt{2} \log 2)!}$$

where t is the thickness in radiation lengths²⁷. A plot of this function for a 10-Mev electron traversing its total range is shown in Figure 10. If ionization losses and variation of the radiative loss with energy are taken into account³⁵, the effect will be to decrease further the low-energy tail. Examination of the energy distribution of the pairs^{9,15} reveals that the low-energy tail will be further decreased; and, consequently, radiative loss at 17-Mev incident x-ray energy will not appreciably affect the resolution. Pairs from a 6-Mev incident x-ray will have negligible loss by radiation.

ELECTRON ESCAPE

Some of the electrons and positrons may escape from the scintillator. In calculating electron escape probability, the electron or positron was assumed to enter scintillator No. 2 at an average angle θ_0 (see Appendix I). The gaussian approximation of Rossi and Greisen²⁷ for the lateral displacement was graphically integrated taking into account the energy loss by collision. The mean square angle of scattering in the gaussian approximation²⁷ is:

$$\frac{E_s^2 t}{2 p^2 \beta^2},$$

where the meaning of the symbols is given in Appendix I. Thus, we find that a 15-Mev electron has an 18 percent probability of escaping with more than 1.5 Mev. Weighting the escape probability with

where θ is the distance in radiation lengths ²⁷. A plot of this function for a 10-Mev electron traversing the total range is shown in Figure 10. It indicates losses and variation of the radiative loss with energy are taken into account²⁸, the effect will be to decrease further the low-energy tail. Examination of the energy distribution of the pairs^{29,30} reveals that the low-energy tail will be further decreased; and, consequently, radiative loss of 17-Mev incident x-ray energy will not appreciably affect the resolution. Pairs from a 6-Mev incident x-ray will have negligible loss by radiation.

ELECTRON SCATTER

Some of the electrons and positrons may escape from the scintillator. In calculating electron escape probability, the electron or positron was assumed to enter scintillator No. 5 at an average angle θ_0 (see Appendix I). The Gaussian approximation of Rossi and Greisen³¹ for the lateral displacement was graphically integrated taking into account the energy loss by scintillation. The mean square angle of scattering in the Gaussian approximation³² is:

$$\frac{\overline{\theta^2}}{2} = \frac{\overline{\theta_0^2}}{2} + \frac{\overline{\theta_1^2}}{2}$$

where the meaning of the symbols is given in Appendix I. Thus, we find that a 17-Mev electron has an 18 percent probability of escape in with more than 1.7 Mev. Weighting the escape probability with

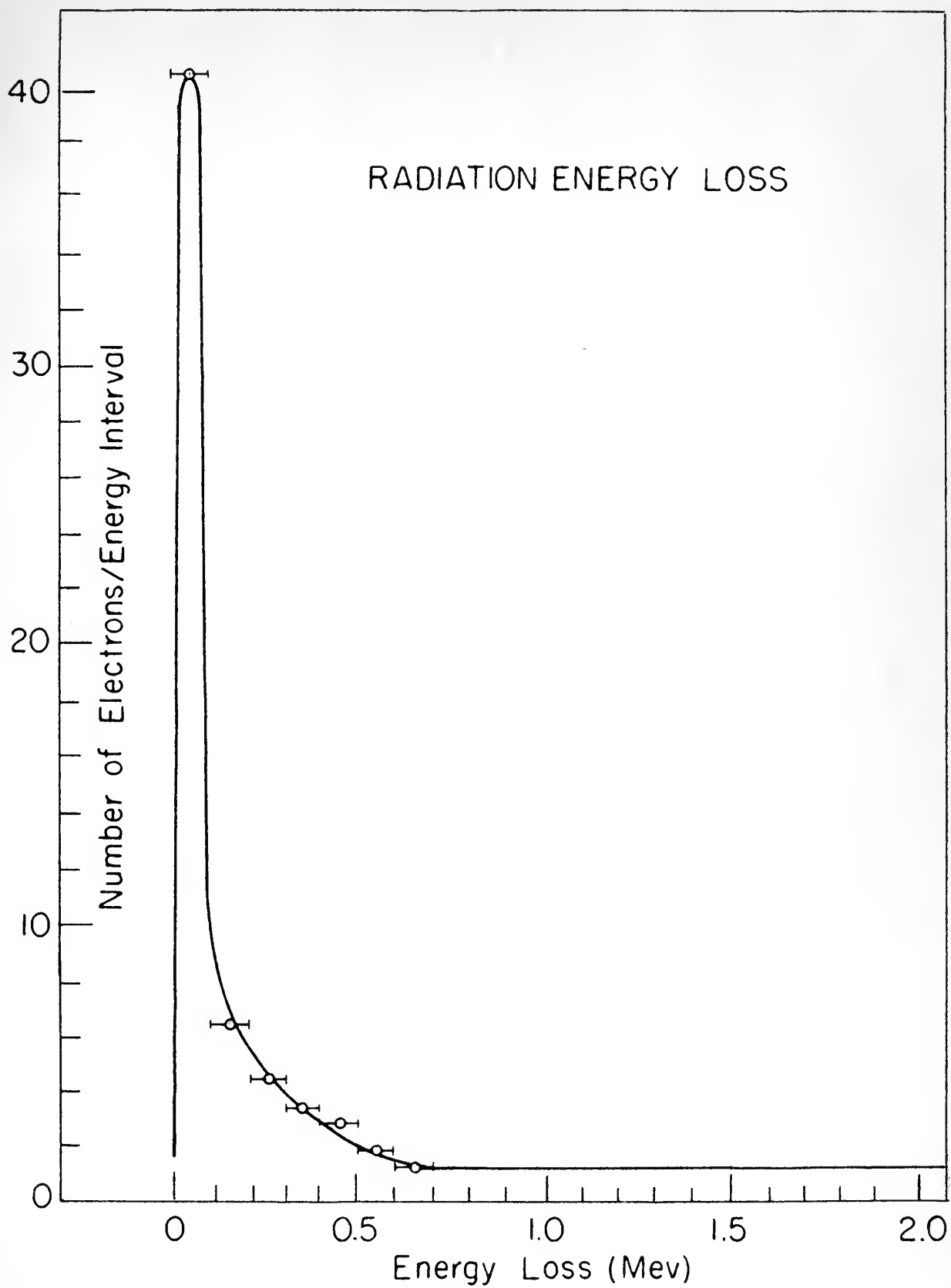
Figure 10

Electron Energy Loss by Radiation

This curve is the differential probability of energy loss by radiation for 100 10-Mev electrons traversing 0.15 radiation lengths in carbon.

Figure 10

Electron Energy Loss by Radiation
This curve is the differential probability
of energy loss by radiation for 100 10-Mev
electrons traversing 0.15 radiation lengths
in carbon.



the pair energy distribution function²⁴ gives the approximate resolution caused by electron escape. This is negligible for a 5-Mev x-ray, of the order of 6 percent for the 17-Mev incident x-ray, and a rapidly increasing function of energy above 15-Mev x-ray energy. The length of scintillator No. 1 is equal to the range³⁶ of a 16-Mev electron.

ENERGY LOSS IN THE CONVERTER

The electron pair created in the converter loses energy in the converter and in the aluminum foil before entering the scintillator. This energy loss is not a constant, and the fluctuations in this energy loss contribute to the energy resolution of the spectrometer. The fluctuation of energy loss occurring when electrons pass through absorbers that are thin compared with their range has been experimentally measured³⁷⁻³⁹ and found to agree with the Landau theory⁴⁰. The net effect of multiple scattering is to increase the relative number of low-energy electrons²⁸. The rms fluctuation in energy loss can be most easily calculated using Yang's Δ correction and assuming the gaussian distribution for the multiple scattering (see Appendix I). Proceeding along these lines, we calculate a root mean square energy loss, which, when divided by the electron energy, gives resolution.

the pair energy distribution function³¹ gives the approximate resolution caused by electron energy. This is negligible for a 2-Mev x-ray, of the order of 6 percent for the 17-Mev incident x-ray, and a rapidly increasing function of energy above 15-Mev x-ray energy. The length of scintillator No. 1 is equal to the range³² of a 16-Mev electron.

ENERGY LOSS IN THE CONVERTER

The electron pair created in the converter loses energy in the converter and in the aluminum foil before entering the scintillator. This energy loss is not a constant, and the fluctuations in this energy loss contribute to the energy resolution of the spectrometer. The fluctuation of energy loss occurring when electrons pass through absorbers that are thin compared with their range has been experimentally measured³⁷⁻³⁹ and found to agree with the Landau theory.⁴⁰ The net effect of multiple scattering is to increase the relative number of low-energy electrons.³⁸ The rms fluctuation in energy loss can be most easily calculated using Yang's correction and assuming the Gaussian distribution for the multiple scattering (see Appendix I). Proceeding along these lines, we calculate a root mean square energy loss, which, when divided by the electron energy, gives resolution.

The aluminum foil used to wrap the scintillator has a total thickness of 3 mils. At 6 Mev, the energy loss calculated as outlined above is of the order of 1 percent; at 17 Mev, this loss is negligible.

The converter can be approximated as an electron point source covered with a foil of half converter thickness. The angular distribution of the electrons in pair production will in general have the same effect as multiple scattering; that is, electrons will not travel a constant straight-line path through the foil but will be distributed in direction (hence, path length) according to the pair production angular distribution. Since a characteristic angle of emission (see Appendix I) is inversely proportional to energy, as also is the root mean square angle of scattering, the ratio of these two angles is roughly independent of energy for a given converter thickness. No gain in resolution can be achieved by reducing the converter thickness beyond the point where the root mean square scattering angle becomes equal to the average angle of pair emission.

Assuming an average electron energy equal to one-half ($E_\gamma - 1.02$), where E_γ is incident x-ray energy in Mev, the following results are obtained for a 16-mil lead converter:

<u>E_γ</u>	<u>Resolution (Percent.)</u>
6	14
11	5.7
17	3.5

The aluminum foil used to wrap the collector has a total thickness of 3 mils. At 6 Mev, the energy loss calculated as outlined above is of the order of 1 percent; at 17 Mev, this loss is negligible.

The converter can be represented as an electron point source covered with a foil of half converter thickness. The angular distribution of the electrons in pair production will in general have the same effect as multiple scattering; that is, electrons will not travel a constant straight-line path through the foil but will be distributed in direction (hence, path length) according to the pair production angular distribution. Since a characteristic angle of emission (see Appendix I) is inversely proportional to energy, as also is the root mean square angle of scattering, the ratio of these two angles is roughly independent of energy for a given converter thickness. No gain in resolution can be achieved by reducing the converter thickness beyond the point where the root mean square scattering angle becomes equal to the average angle of pair emission.

Assuming an average electron energy equal to one-half $(E_\gamma - 1.02)$, where E_γ is incident x-ray energy in Mev, the following results are obtained for a 16-mil lead converter:

E_γ	Resolution (percent)
6	16
11	2.7
17	3.2

The effect of radiation loss in the converter is smaller than the above.

CAPTURE OF ANNIHILATION QUANTA

Capture of an appreciable fraction of the annihilation quanta in the scintillator will impair the energy resolution of the spectrometer.

The fraction of gamma-ray energy dissipated by a narrow beam in passing through the scintillator is not the same as the fractional loss of intensity. It is necessary to multiply the probability of each interaction process (Compton and photoelectric) by the probable fraction of the photon energy actually dissipated in the absorber as a result of the process. Using this method, one takes the value of the energy absorption coefficient to be $0.029 \text{ cm}^2/\text{gm}$ at 0.51 Mev for "Pilot B" scintillators (Fano⁴¹).

The method used to calculate the probability that at least one annihilation quantum is absorbed is as follows: Assume an average angle of pair emission and that the range of the electron¹⁸ is approximately that for aluminum. (The energy loss in mica, carbon, and air is not significantly different from that in the same weight of aluminum³³.) From this stopping point, assuming the quanta are isotropically emitted back-to-back with equal energies²¹, we establish an average solid angle and an average path length. From this

The effect of radiation loss in the converter is smaller than

the above.

CALCULATION OF ANNIHILATION QUANTA

Calculation of an approximate fraction of the annihilation quanta

in the scintillator will require the energy resolution of the spec-

troscopy.

The fraction of gamma-ray energy dissipated by a narrow beam in passing through the scintillator is not the same as the fractional

loss of intensity. It is necessary to multiply the probability of

each interaction process (Compton and photoelectric) by the probability

fraction of the photon energy actually dissipated in the absorber as

a result of the process. Using this method, one takes the value of

the energy absorption coefficient to be 0.039 cm²/gm at 0.511 Mev for

"Pilot B" scintillators (Lanex).

The method used to calculate the probability that at least

one annihilation quantum is absorbed is as follows: Assume an aver-

age angle of pair emission and that the range of the electron is

approximately that for aluminum. (The energy loss in lead, carbon,

and air is not significantly different from that in the same weight

of aluminum.) From this stopping point, assuming the quanta are

isotropically emitted back-to-back with equal energies²¹, we calcu-

late an average solid angle and an average path length. From this

is calculated the average energy absorbed by the scintillator, taking into account the energy distribution function of the pair electrons. At 17 Mev, about 4 percent of the annihilation quanta are absorbed in the scintillator and about 7 percent are absorbed at 6 Mev.

SUMMARY OF EXPECTED RESOLUTION

To summarize this chapter, assuming that the processes above are statistically independent²², one arrives at the following values for the expected resolution of the spectrometer when using a 16-mil lead converter:

<u>E_γ</u>	<u>Resolution</u> <u>(Percent.)</u>
6	20
10	12
17	10

is calculated the average energy absorbed by the scintillator, taking into account the energy distribution function of the pair electrons. At 17 Mev, about 1 percent of the annihilation quanta are absorbed in the scintillator and about 7 percent are absorbed at 6 Mev.

SUMMARY OF EXPECTED RESOLUTION

To summarize this chapter, assuming that the processes above are statistically independent, one arrives at the following values for the expected resolution of the spectrometer when using a 16-mil lead converter:

E_γ	Resolution (Percent)
6	30
10	18
17	10

VI. CALIBRATION AT THE ROCKEFELLER GENERATOR

The spectrometer is calibrated by using two gamma-rays of known energies to provide the two points necessary to draw the linear characteristics⁹⁻¹¹ of the scintillator. Since there are no available monoenergetic gamma sources about 5 Mev, it is necessary to utilize gamma-rays from nuclear reactions. The source of gamma-rays generally used for this type of work is from the proton bombardment of light elements.

The source of protons for testing the spectrometer was the M.I.T. Rockefeller electrostatic generator. This generator is capable of delivering a magnetically analyzed (to within 0.1 percent) proton beam of 5 microamperes, continuously variable from 0.7 to 4 Mev. The output proton current is determined by a proton beam current integrator. The area of the proton beam at the target is about 4 square millimeters, so that for the purposes of this experiment the gamma-ray originates from a point source. Figure 11 shows a photograph of the spectrometer and proton target. A scale drawing showing distances from the source is given in Figure 1.

In view of the difficulty of preparing thin proton targets that will physically withstand high proton bombardment current, it was decided to use thick targets. Targetholders were made of 10-mil aluminum disks 2 inches in diameter. A 1/16 inch deep 1/2 inch

VI. CALIBRATION AT THE ROSENBLUTH GENERATOR

The spectrometer is calibrated by using two gamma-rays of known energies to provide the two points necessary to draw the linear characteristics²⁻¹¹ of the scintillator. Since there are no available monochromatic gamma sources about 2 Mev, it is necessary to utilize gamma-rays from nuclear reactions. The source of gamma-rays generally used for this type of work is from the proton bombardment of light elements.

The source of protons for testing the spectrometer was the H.I.T. Rosenbluth electrostatic generator. This generator is capable of delivering a magnetically analyzed (to within 0.1 per cent) proton beam of 2 microns, continuously variable from 0.7 to 1 Mev. The output proton current is determined by a proton beam current integrator. The area of the proton beam at the target is about 1 square millimeter, so that for the purposes of this experiment the gamma-ray originates from a point source. Figure 11 shows a photograph of the spectrometer and proton target. A scale drawing showing distances from the source is given in Figure 1.

In view of the difficulty of preparing thin proton targets that will physically withstand high proton bombardment current, it was decided to use thick targets. Targets were made of 10-12 mil aluminum disks 2 inches in diameter. A 1/16 inch deep 1/8 inch

Figure 11

The Spectrometer in Place at the MIT Rockefeller Generator

This figure is a photograph of the spectrometer at the Rockefeller generator as it was located for testing and calibration. The proton target is shown in the right of the photograph.

Figure 11

The spectrometer in place at the MIT Rockwell generator

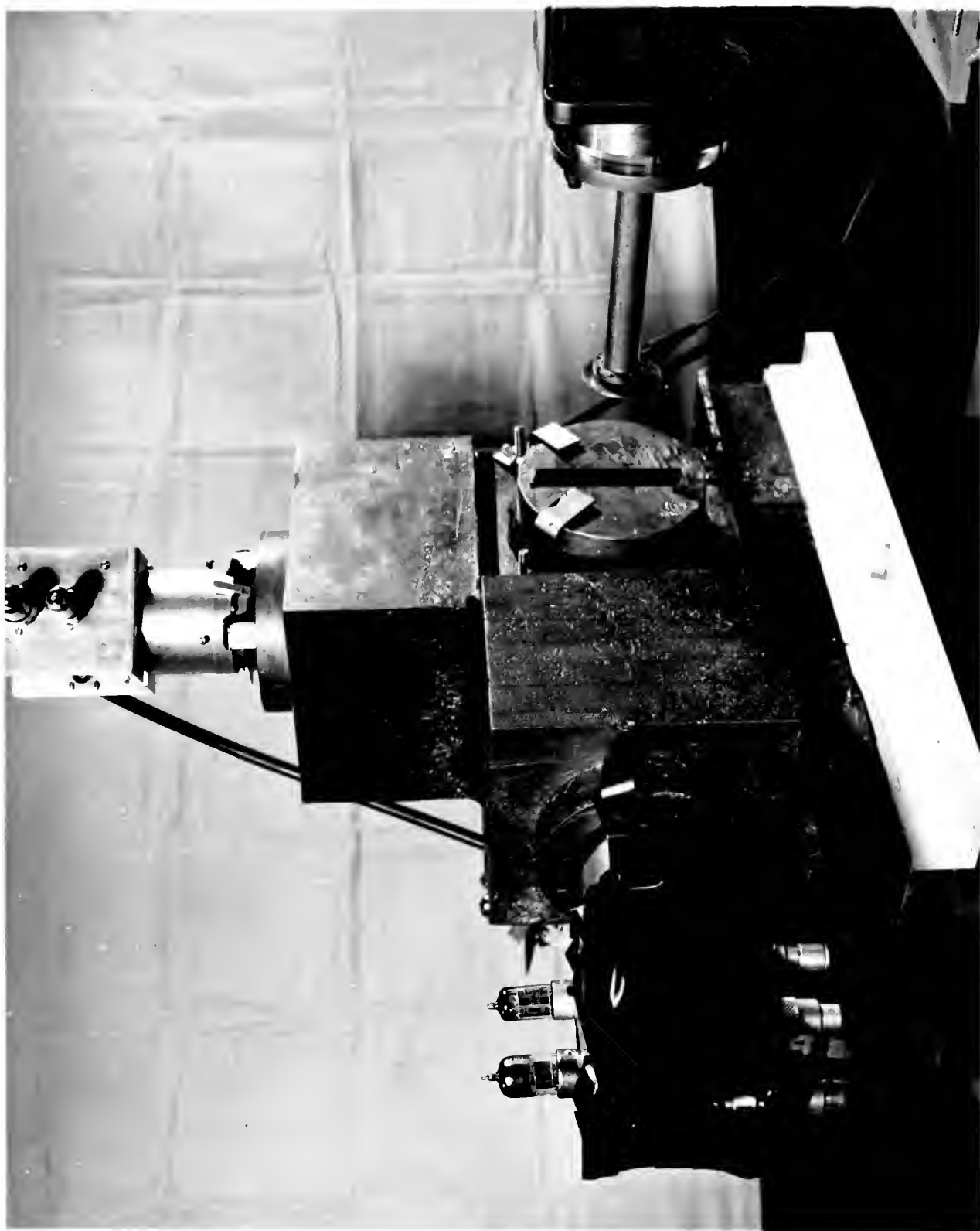
This figure is a photograph of the spec-

trometer at the Rockwell generator as

it was located for testing and calibra-

tion. The proton target is shown in the

right of the photograph.



diameter recess was formed in the center of the aluminum disk to hold the target material. Using the same die used to make the depression, the target material was pressed into the recess. This method proved satisfactory for all materials other than boron. The B_4C sample was obtained through the courtesy of Professor J. T. Norton, Metallurgical Department, M. I. T. It was in the form of a 3/16 inch thick sample, hot pressed in a graphite die.

A list of energy standards used and references giving the yields and gamma-ray energies follows:

TABLE II

<u>Target Material</u>	<u>Proton Bombardment Energy (Mev)</u>	<u>Gamma Energy (Mev)</u>	<u>Yield ($\gamma/10^9$ Protons)</u>	<u>Reference</u>
B_4C	1.2	16.7	2	12
		12.12	4	12
		4.41	4	12
CaF	1.15	6.13	500	4,12
		7.0	200	4,12
Li Metal	1.15	17.6	20	4,16
		14.8	30	4,16

To a first approximation, the counting rate of the spectrometer is the fraction of solid angle subtended times the probability

A list of energy standards used and references giving the yields and gamma-ray energies follows:

A $3/16$ inch thick sample, hot pressed in a graphite die. Norton, Metallurgical Department, M. I. T. It was in the form of a H_2O sample was obtained through the courtesy of Professor J. T. method proved satisfactory for all materials other than boron. This deposition, the target material was pressed into the recess. This hold the target material. Using the same die used to make the diameter recess was formed in the center of the aluminum disk to

TABLE II

Reference	Yield ($\gamma/10^9$ Protons)	Gamma Energy (MeV)	Proton Bombardment Energy (MeV)	Target Material
12	2	16.7	1.2	H_2O
12	11	12.12		
12	11	11.11		
12, 12	200	6.13	1.12	CaF
12, 12	200	7.0		
12, 12	20	17.6	1.12	Al metal
12, 12	30	11.8		

After is the fraction of solid angle subtended times the probability
To a first approximation, the counting rate of the spectrum-

of producing a pair in the converter times the rate of emission of gamma radiation. The actual efficiency of the counter must be determined by experiment, since the efficiency is an unknown function of D2 and D1 settings, as well as the incident x-ray energy.

Taking into consideration target conditions, pair cross section, and solid angle which obtain at the Rockefeller generator, it was determined that the approximate times to record 1000 counts are as follows:

<u>Target</u>	<u>Time</u>
CaF	10 min
Li	1 hour
B ₄ C	1 hour

The danger of contaminating the Rockefeller generator imposes a proton current limitation when bombarding lithium targets; this limitation is not present with B₄C. This fact, coupled with the formation of LiOH at the surface, reduces the maximum attainable lithium yield by about a factor of 10, which effectively gives the same obtainable counting rate for lithium and boron.

of producing a pair in the converter times the rate of emission of gamma radiation. The actual efficiency of the counter must be determined by experiment, since the efficiency is an unknown function of E and E_0 settings, as well as the incident x-ray energy. Taking into consideration target conditions, pair cross section, and solid angle which obtain at the Rockwell generator, it was determined that the approximate times to record 1000 counts are as follows:

Target	Time
Co	10 min
Li	1 hour
Bi	1 hour

The danger of contaminating the Rockwell generator imposes a proton current limitation when considering lithium targets; this limitation is not present with ^{60}Co . This fact, coupled with the fact that the maximum attainable lithium yield by about a factor of 10, which effectively gives the same attainable counting rate for lithium and bismuth.

VII. DISCUSSION OF EXPERIMENTAL RESULTS

ENERGY CALIBRATION

The calibration of the spectrometer is in terms of the pulser voltage. The raw data are, however, recorded in terms of channel number. The channel number (C) is related to voltage by:

$$C = f(V_{1a} + K'V_{2a}) \quad (1)$$

where V_{1a} and V_{2a} are input pulse heights in volts to the addition circuit from units Nos. 1 and 2, respectively; K' is an amplification factor determined by the parameters of the addition circuit. Assuming linearity as far as the addition circuit, equation (1) may be written:

$$C = g(V)$$

where $V = 3(V_1 + KV_2)$; V_1 and V_2 are the output voltage of scintillation units Nos. 1 and 2, respectively. V is a pulser voltage, and the factor of 3 comes from the parameters of the circuit in which pulser and photomultiplier signals are mixed.

A typical calibration curve, giving $C = g(V)$, is shown in Figure 12. The calibration curve is measured both with $V_2 = 0$ and $V_1 = V_2$ in order to determine the addition factor K . The value of K ordinarily used was 0.450 and was stable to 0.5 percent for several hours. The nonlinearity at the upper end of the curve shown in

VII. DISCUSSION OF EXPERIMENTAL RESULTS

ENERGY CALIBRATION

The calibration of the spectrometer is in terms of the pulse voltage. The raw data are, however, recorded in terms of channel number. The channel number (C) is related to voltage by:

$$C = f(V) = K_1 V + K_2 V^2 \quad (1)$$

where V_1 and V_2 are input pulse heights in volts to the addition circuit from units Nos. 1 and 2, respectively; K_1 is an amplification factor determined by the parameters of the addition circuit. Assuming linearity as far as the addition circuit, equation (1) may be written:

$$C = f(V)$$

where $V = V_1 + K_2 V_2$, V_1 and V_2 are the output voltage of addition circuit with Nos. 1 and 2, respectively. V is a pulse voltage, and the factor of 3 comes from the parameters of the circuit in which pulse and photomultiplier signals are mixed.

A typical calibration curve, giving $C = f(V)$, is shown in Figure 12. The calibration curve is measured both with $V_2 = 0$ and $V_1 = V$ in order to determine the addition factor K_2 . The value of K_2 ordinarily used was 0.450 and was stable to 0.2 percent for several hours. The nonlinearity at the upper end of the curve shown in

Figure 12

Calibration Curve

Shown here is a typical calibration curve made before, during, and after each run.

Raw data are in the form of counts per channel as a function of channel number. Data are converted into counts per volt as a function of pulser voltage.

Figure 13

Calibration Curve

Shown here is a typical calibration curve made before, during, and after each run. Raw data are in the form of counts per channel as a function of channel number. Data are converted into counts per volt as a function of pulse voltage.

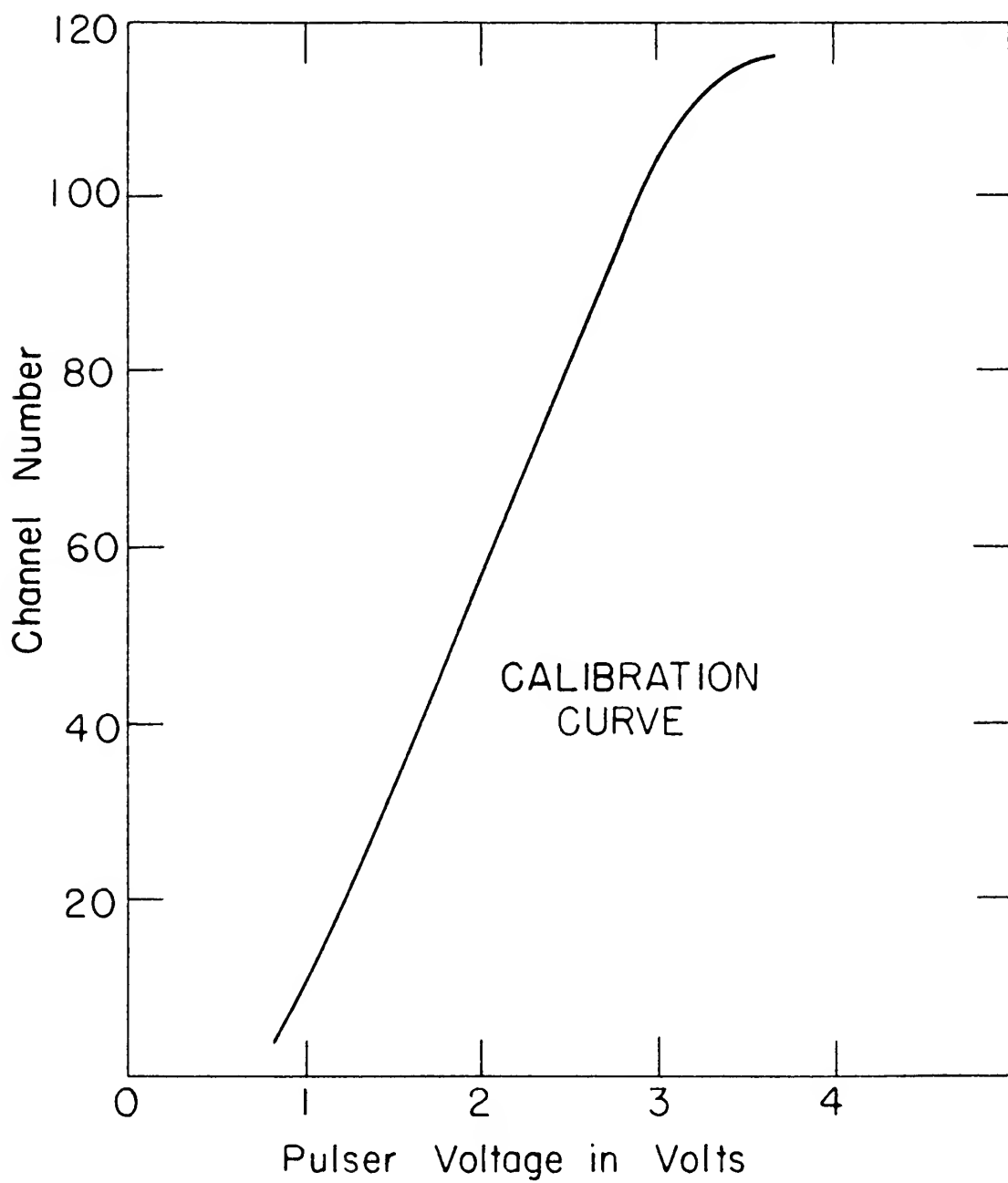


Figure 12 comes from overloading the stage of amplification just before the pulse-height analyzer. The nonlinearity in the lower part of the curve comes from diode nonlinearity in the pulse-height analyzer.

The energy of the incident x-ray is:

$$E_{\gamma} = 1.02 + E_1 + E_2 + E_0 ,$$

where E_1 and E_2 are energy losses (in Mev) in scintillators Nos. 1 and 2, respectively, and E_0 is the most probable energy lost by electrons and positrons in the lead converter (about 0.5 Mev).

$$V = \frac{V_1}{E_1} E_1 + K \frac{V_2}{E_2} E_2 .$$

The ratios V_1/E_1 may be controlled by varying the photomultiplier high voltage.

The same negative power supply furnished the high voltage for No. 1 and No. 2. This supply was stable to 0.1 percent for periods of several hours. Both photomultipliers were operated at -740 volts.

Calibration was accomplished by varying the addition factor, K , until the peaks from the 6-Mev fluorine line and the 16-Mev $B_{11}C$ line fell in the correct relative positions (see Figure 13).

Figure 12 comes from overloading the stage of amplification just before the pulse-height analyzer. The nonlinearity in the lower part of the curve comes from diode nonlinearity in the pulse-height analyzer.

The energy of the incident x-ray is

$$E_0 = 1.02 + E_1 + E_2 + E_3$$

where E_1 and E_2 are energy losses (in Mev) in scintillation Nos. 1 and 2, respectively, and E_3 is the most probable energy lost by electrons and positrons in the lead converter (about 0.2 Mev).

$$V = \frac{E_1}{E_2} \frac{V_1}{V_2} + K \frac{V_3}{E_2}$$

The ratios V_1/V_2 may be controlled by varying the photomultiplier high voltage.

The same negative power supply furnished the high voltage for Nos. 1 and No. 2. This supply was stable to 0.1 percent for periods of several hours. Both photomultipliers were operated at -750 volts.

Calibration was accomplished by varying the addition factor, K , until the peaks from the 6-Mev fluorine line and the 15-Mev H_{10}^+ line fell in the correct relative positions (see Figure 13).

Figure 13

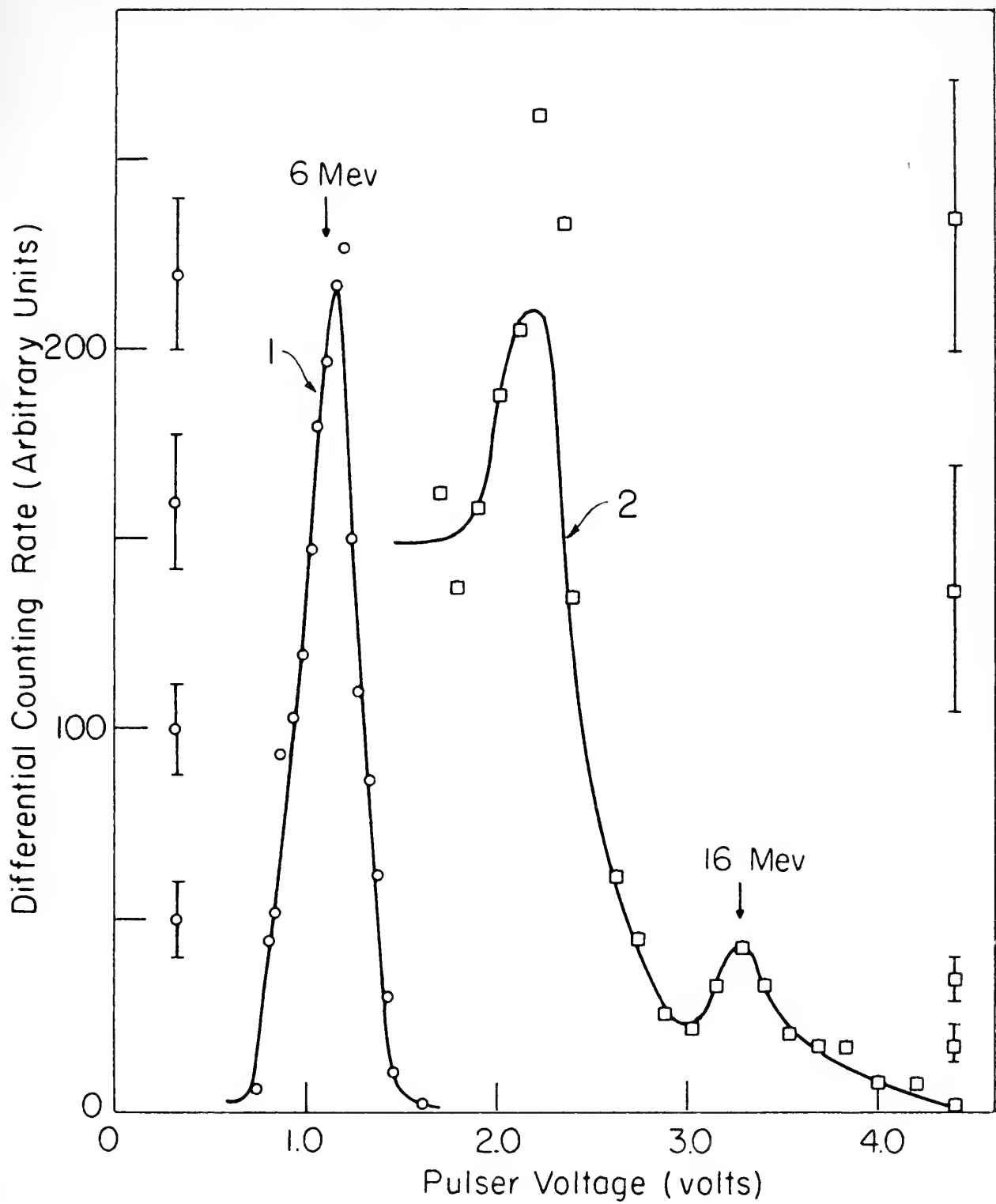
Energy Calibration

Curve No. 1 was obtained by proton bombardment of a thick CaF target; curve No. 2 by proton bombardment of a thick B_4C target. A 16-mil lead converter was used for both curves. The boron curve (No. 2) from 1.5 - 2.5 volts was obtained with poor statistics and normalized to match the 2.5 - 4.5 volt section. There is some evidence of the 12-Mev line at 2.3 volts. The anticoincidence circuit had not been designed when these runs were made.

Figure 11

Energy Calibration

Curve No. 1 was obtained by proton bombardment of a thick Cu target; curve No. 2 by proton bombardment of a thick B₂O₃ target. A 15-mil lead converter was used for both curves. The boron curve (No. 2) from 1.5 - 3.5 volts was obtained with poor statistics and not unlike to match the 3.5 - 4.5 volt section. There is some evidence of the 15-Mev line at 3.3 volts. The anticoincidence circuit had not been designed when these runs were made.



FLUORINE RUNS

The low-energy limitation of the spectrometer is imposed by the rapid decrease of the pair production cross section with decreasing energy, combined with the increase in Compton cross section. At about 5 Mev (where these two cross sections are about equal), the resolution of the spectrometer is limited by the inability of discriminator No. 2 to perform its designed function; that is, separation of the doubly ionizing pulses of the pair process from the singly ionizing pulses of the Compton recoil electrons. Figure 14 illustrates the lack of a definite separation between pairs and Compton recoil electrons for 6-Mev incident x-ray energy. A sufficiently thin converter with a very thin scintillator No. 2 would perform this function at, say, 3 Mev, since multiple scattering in the converter and in the scintillator, with consequent increased fluctuations in the energy loss, would be minimized. A point is reached, however, where light collection difficulties and photomultiplier statistics impose a lower energy limit to the usefulness of the spectrometer.

Figure 15 illustrates the effect of changes in spectrum shape with changes in D1. In order for the spectrometer to function, it is necessary that there be a region where changing D1 does not materially affect spectrum shape. Figure 15 illustrates that such a plateau does in fact exist; that is, changing D1 from very

DISCUSSION

The low-energy limitation of the spectrometer is imposed by

the rapid decrease of the pair production cross section with de-
creasing energy, combined with the increase in Compton cross sec-
tion. At about 2 Mev (where these two cross sections are about

equal), the resolution of the spectrometer is limited by the
instability of discriminator No. 2 to perform its designed function;
that is, separation of the doubly ionizing pulses of the pair prod-
ucts from the singly ionizing pulses of the Compton recoil electrons.

Figure 11 illustrates the lack of a definite separation between
pair and Compton recoil electrons for 6-Mev incident x-ray energy.

A sufficiently thin converter with a very thin scintillator No. 2
would perform this function at, say, 3 Mev, since multiple scatter-
ing in the converter and in the scintillator, with consequent in-
creased fluctuations in the energy loss, would be minimized. A

point is reached, however, where light collection difficulties and
photomultiplier statistics impose a lower energy limit to the use-
fulness of the spectrometer.

Figure 12 illustrates the effect of changes in spectrum
shape with changes in D1. In order for the spectrometer to func-
tion, it is necessary that there be a region where changing D1 does
not materially affect spectrum shape. Figure 12 illustrates that
such a plateau does in fact exist; that is, changing D1 from very

Figure 14

Pulse-Height Distribution for Scintillator No. 2 at 6 Mev

This curve was obtained by the proton bombardment of a thick CaF target using a 16-mil lead converter. The standard statistical errors of the points are indicated to the right of the curve.

Figure 11

Figure 11 shows the distribution for the test of the null hypothesis that the mean of the distribution is equal to zero. The curve was obtained by the method of moments of a thick tail target using a 10-ml lead container. The standard statistical errors of the points are indicated to the right of the curve.

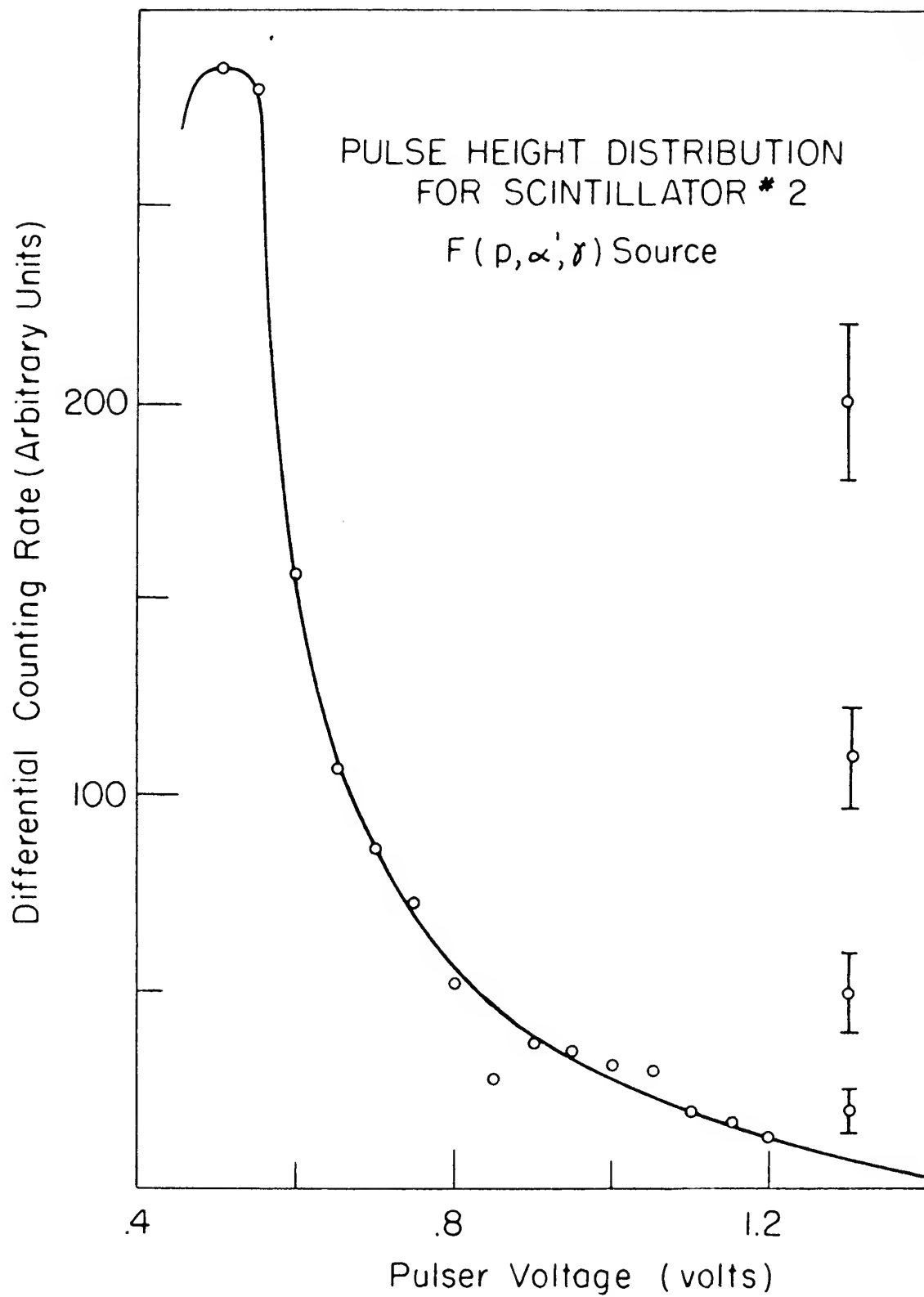


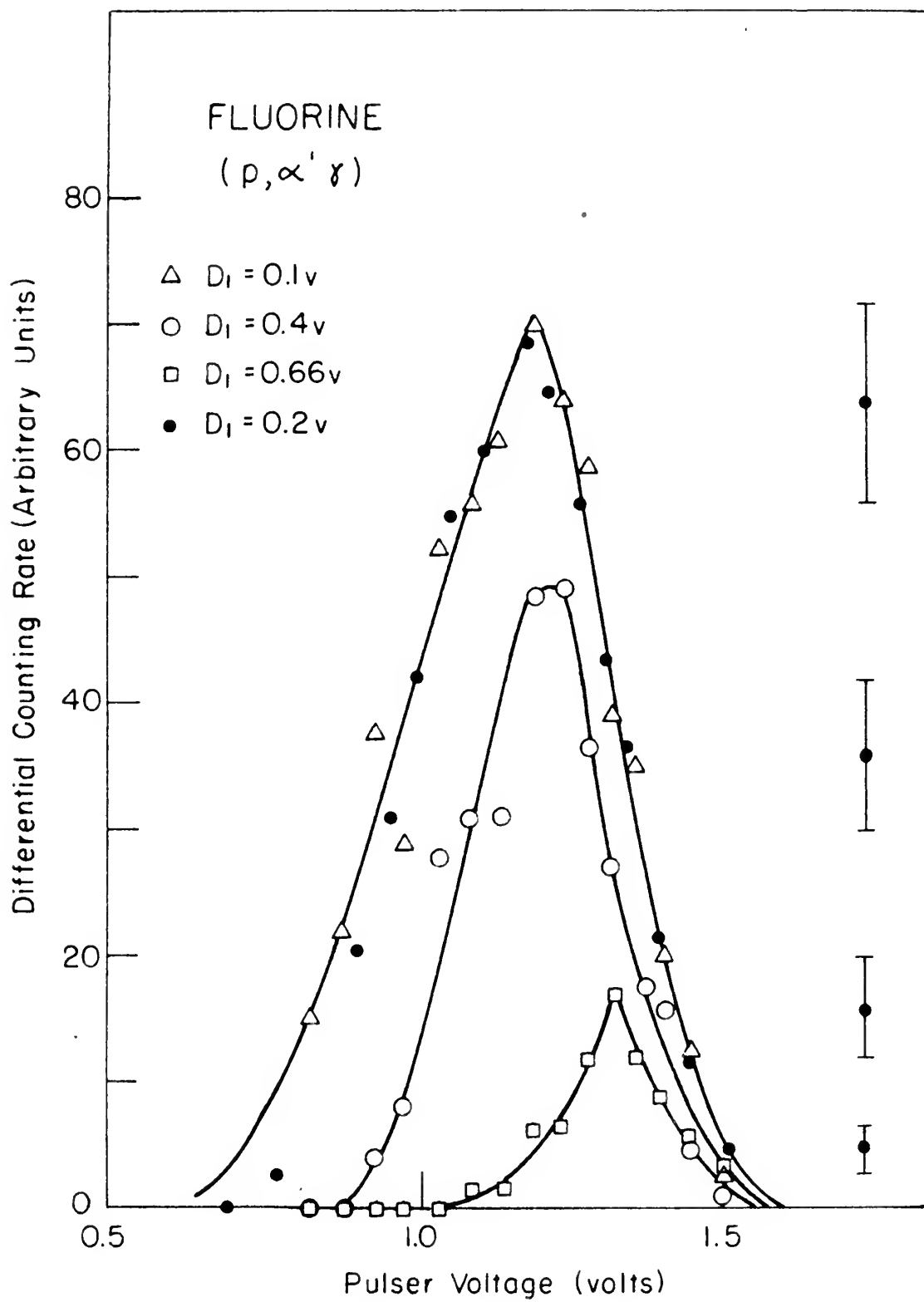
Figure 15

Effect of Changing Discriminator No. 1

All curves in this figure were obtained by proton bombardment of a thick CaF target using a 16-mil lead converter. These curves are normalized to the same number of protons incident on the target.

Figure 12

Effect of Changing Discriminator No. 1
All curves in this figure were obtained
by proton bombardment of a thick Ge
target using a 15-mil lead converter.
These curves are normalized to the same
number of protons incident on the target.



low to 0.2 volts does not affect the position of the peak or the resolution. D1 at 0.2 volts requires at least 1-Mev energy loss in scintillator No. 1.

Figure 16 illustrates the change in efficiency of the spectrometer with changes in the setting of discriminator No. 2 at 6-Mev incident x-ray energy. These curves were all made with the same setting of D1; that is, 0.2 volts, and normalized to the same number of protons incident on the $F^{19}(p,\alpha'\gamma)$ target. Hence, the ratio of the areas under the curves of Figure 16 gives directly the ratio of spectrometer efficiency for the given discriminator settings. These ratios are 1:2:3.8, in agreement with the shape of the distribution curve for scintillator No. 2 shown in Figure 11. The curve for D2 = 0.8 volts corresponds to an efficiency of 8×10^{-3} for 6-Mev incident x-ray energy, 16-mil lead converter.

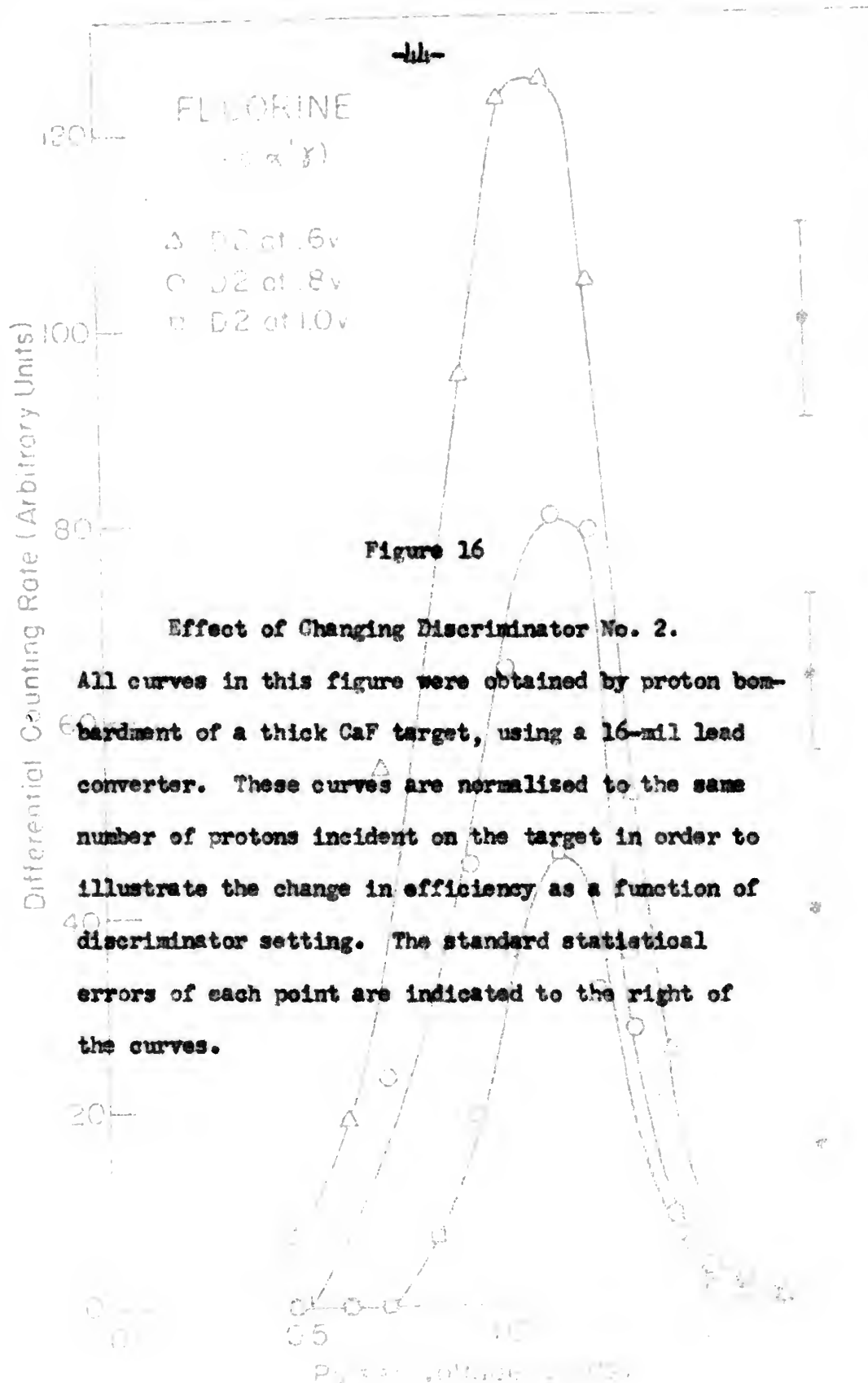
Considering the contribution of the 7-Mev fluorine line, the resolution at 6 Mev is about 25 percent, which is about the resolution predicted in Chapter V. The lowest energy at which the present spectrometer is useful is 6 Mev. To reduce this limit, to improve the resolution at 6 Mev, and perhaps more important to obtain a better plateau of efficiency as a function of D2 would require a thinner lead converter and a thinner scintillator No. 2.

low to 0.2 volts does not affect the position of the peak or the resolution. DI at 0.2 volts requires at least 1-kev energy loss in scintillator No. 1.

Figure 16 illustrates the change in efficiency of the spectrometer with changes in the setting of discriminator No. 2 at 6-kev incident x-ray energy. These curves were all made with the same setting of DI; that is, 0.2 volts, and normalized to the same number of protons incident on the $P(p, \alpha, \gamma)$ target. Hence, the ratio of the areas under the curves of Figure 16 gives directly the ratio of spectrometer efficiency for the given discriminator settings.

These ratios are 1:1.3:1.8, in agreement with the shape of the distribution curves for scintillator No. 2 shown in Figure 15. The curves for DI = 0.2 volts corresponds to an efficiency of 8×10^{-3} for 6-kev incident x-ray energy, 16-mil lead converter.

Considering the contribution of the 7-kev line, the resolution at 6 kev is about 2% percent, which is about the resolution predicted in Chapter V. The lowest energy at which the present spectrometer is useful is 6 kev. To reduce this limit, to improve the resolution at 6 kev, and perhaps more important to obtain a better picture of efficiency as a function of E would require a thinner lead converter and a thinner scintillator No. 2.



low to 0.2 volts does not affect the position of the peak or the resolution. DI at 0.5 volts requires at least 1-Mev energy loss in

scintillator No. 1.

Figure 16 illustrates the change in efficiency of the spectrometer with changes in the setting of discriminator No. 2 at 6-Mev

incident x-ray energy. These curves were all made with the same setting of DI; that is, 0.5 volts, and normalized to the same number of protons incident on the Y_2O_3 target. Hence, the ratio of the areas under the curves of Figure 16 gives directly the ratio

of spectrometer efficiency for the given discriminator settings. These ratios are 1:2:3.8, in agreement with the shape of the distribution

curve for scintillator No. 2 shown in Figure 16. The curve for DI = 0.8 volts corresponds to an efficiency of 8×10^{-3} for

6-Mev incident x-ray energy, 16-Mev lead converter.

Considering the contribution of the 7-Mev fluorine line, the resolution at 6 Mev is about 25 percent, which is about the present limit predicted in Chapter V. The lowest energy at which the present spectrometer is useful is 6 Mev. To reduce this limit, to improve

the resolution at 6 Mev, and perhaps more important to obtain a better picture of efficiency as a function of E would require a

thinner lead converter and a thinner scintillator No. 2.

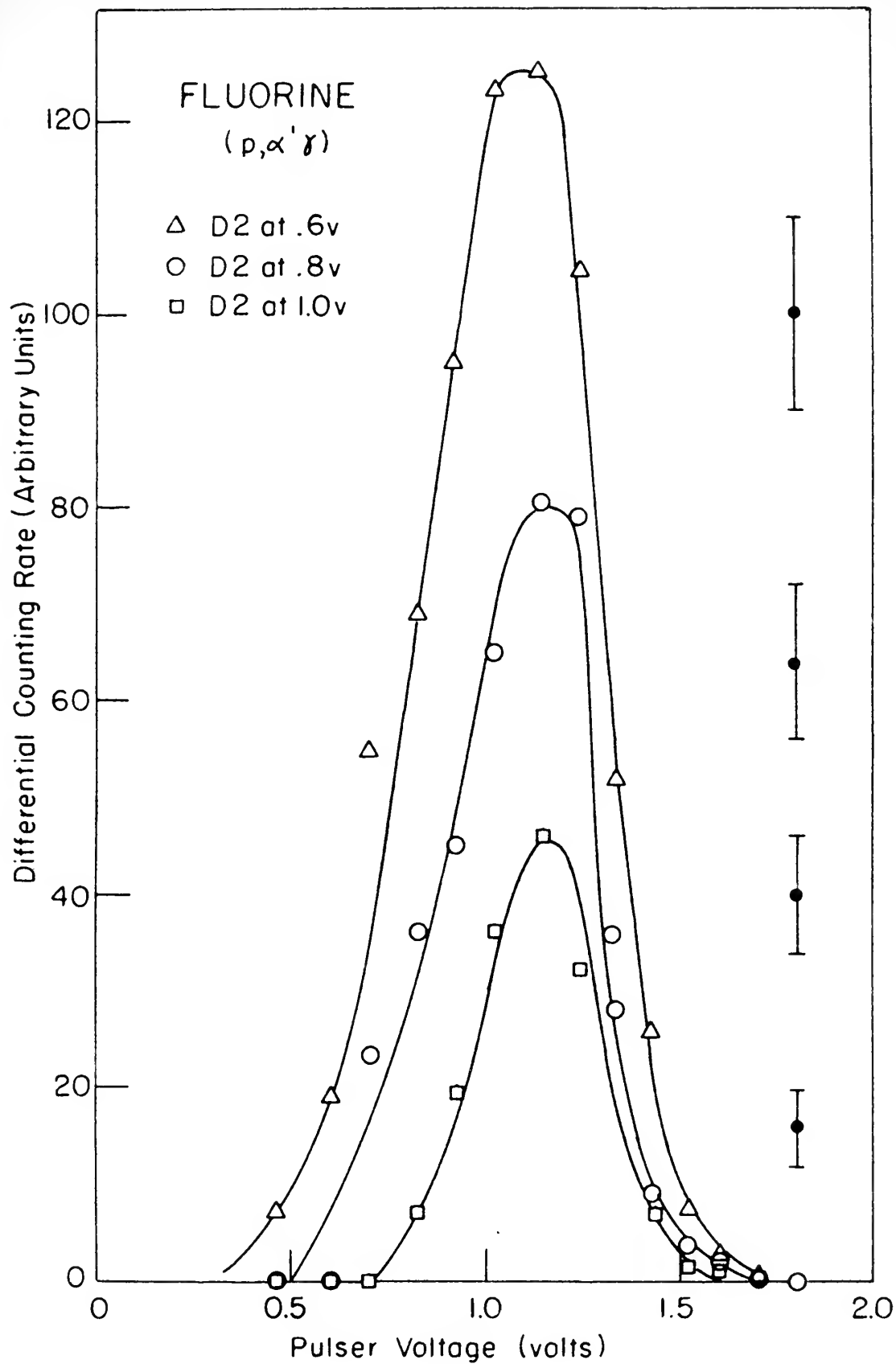
Figure 16

Effect of Changing Discriminator No. 2.

All curves in this figure were obtained by proton bombardment of a thick CaF target, using a 16-mil lead converter. These curves are normalized to the same number of protons incident on the target in order to illustrate the change in efficiency as a function of discriminator setting. The standard statistical errors of each point are indicated to the right of the curves.

Figure 10

Effect of Changing Discriminator No. 2.
All curves in this figure were obtained by proton bombardment of a thick Ge target, using a 10-mil lead converter. These curves are normalized to the same number of protons incident on the target in order to illustrate the change in efficiency as a function of discriminator setting. The standard statistical errors of each point are indicated to the right of the curves.



HIGH-ENERGY RUNS

The difficulties apparent in the high-energy region, as illustrated by Figure 13, led to the necessity for design of the anticoincidence circuit. Figure 17 illustrates the difficulty in distinguishing singly and doubly ionizing events with the anticoincidence scintillator out of the circuit. This figure also demonstrates the apparent success of scintillator No. 3 in eliminating high background effects which mask the expected doubly ionizing peak calculated and shown on Figure 9 of Chapter III. To date, the only runs made with the anticoincidence unit in operation were the pulse-height distribution in scintillator No. 2 shown in Figure 17.

The prediction in Chapter V regarding electron escape and radiation loss from scintillator No. 1 should be experimentally verified by a high-energy electron source. The high-energy limit of the spectrometer is imposed as a result of rapidly increasing electron escape probability with increasing energy above 15 Mev.

HIGH-ENERGY RIMS

The differential spectrum in the high-energy region, as illustrated by Figure 1, led to the necessity for design of the coincidence circuit. Figure 17 illustrates the difficulty in distinguishing singly and doubly ionizing events with the anticoincidence scintillator out of the circuit. This figure also demonstrates the apparent success of scintillator No. 3 in eliminating high background effects which mask the expected doubly ionizing peak calculated and shown on Figure 9 of Chapter III. To date, the only runs made with the anticoincidence unit in operation were the pulse-height distribution in scintillator No. 3 shown in Figure 17.

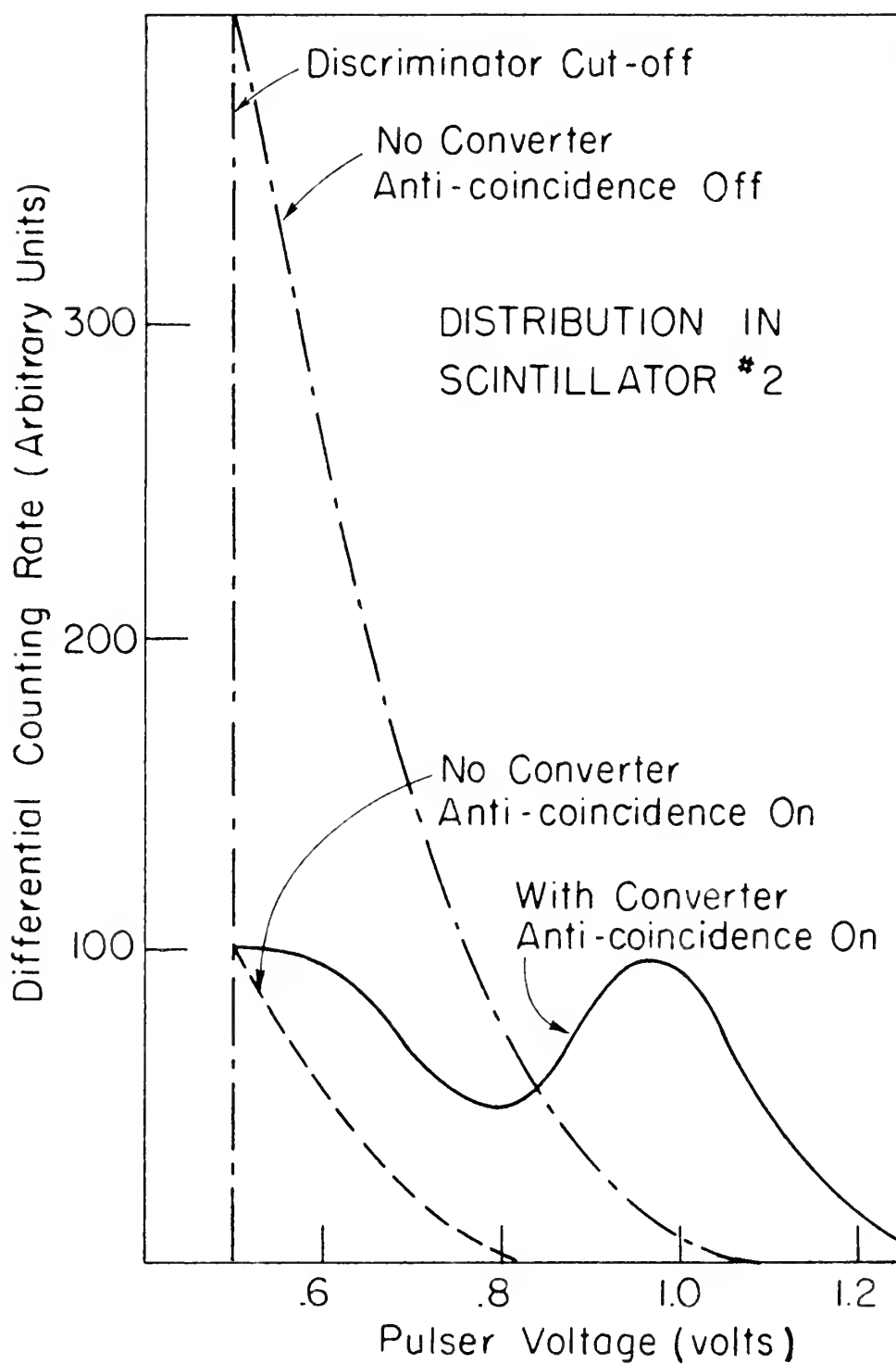
The prediction in Chapter V regarding electron escape and radiation loss from scintillator No. 1 should be experimentally verified by a high-energy electron source. The high-energy limit of the spectrometer is imposed as a result of rapidly increasing electron escape probability with increasing energy above 15 Mev.

Figure 17

Effect of the Anticoincidence Circuit at 17 Mev
The curves shown were obtained by proton bombardment of a thick lithium metal target, using a 16-mil lead converter. The need for the anticoincidence circuit at high x-ray energy is illustrated.

Figure 17

Effect of the Antineutrino Circuit at 17 Mev
 The curves shown were obtained by proton bombardment
 of a thick lithium metal target, using a 16-Mv lead
 converter. The need for the antineutrino circuit
 at high x-ray energy is illustrated.



VIII. SUMMARY

An attempt has been made to design, instrument, and calibrate an x-ray scintillation pair spectrometer capable of 10 percent resolution at 10 Mev. The spectrometer is designed for use at the M. I. T. linear accelerator and consequently must span the 5- to 17-Mev x-ray energy region. This three scintillator telescope arrangement relies on the ability of a thin plastic scintillator to distinguish the doubly ionizing pulses originating in the thin lead converter as a result of the pair process.

Careful study of the 6-Mev fluorine gamma-ray has shown:

1. That the observed resolution of 20 to 25 percent is in agreement with predicted values for the thickness of the lead converter and plastic scintillator used;
2. That coincidence pulses are doubly ionizing events, and;
3. Better resolution can be obtained by using a thinner lead converter and thinner plastic scintillator No. 2.

Study of the high-energy incident x-ray region, using the 17-Mev lithium gamma-ray, demonstrated that an anticoincidence circuit was necessary to distinguish doubly ionizing events. Subsequent experimental observations of the pulse height distribution in scintillator No. 2 pointed to the apparent success of the anticoincidence circuit. A program similar to that performed at 6 Mev remains to be carried out at 17 Mev to determine optimum operating conditions in this energy region.

VIII. SUMMARY

An attempt has been made to design, construct, and calibrate an x-ray scintillation pair spectrometer capable of 10 percent resolution at 10 Mev. The spectrometer is designed for use at the M. I. T. linear accelerator and consequently must span the 5- to 15-Mev x-ray energy region. This three scintillator telescope arrangement relies on the ability of a thin plastic scintillator to distinguish the doubly ionizing pulses originating in the thin lead converter as a result of the pair process.

Careful study of the 6-Mev fluorine gamma-ray has shown:

1. That the observed resolution of 30 to 35 percent is in agreement with predicted values for the thickness of the lead converter and plastic scintillator used;

2. That coincident pulses are doubly ionizing events,

and;

3. Better resolution can be obtained by using a thinner

lead converter and thinner plastic scintillator No. 5.

Study of the high-energy incident x-ray region, using the 15-Mev lithium gamma-ray, demonstrated that an anticoincidence circuit was necessary to distinguish doubly ionizing events. Subsequent experimental

observations of the pulse height distribution in scintillator No. 5 pointed to the apparent success of the anticoincidence circuit. A program similar to that performed at 6 Mev remains to be carried out in order to determine optimum operating conditions in this energy region.

APPENDIX I

CALCULATION OF DIFFERENTIAL ENERGY LOSS DISTRIBUTION FOR SCINTILLATOR No. 2 AT 17.6-Mev INCIDENT X-RAY ENERGY

Using the electron energy distributions given by Johns et al.²⁴ in tabulated form for 1-Mev energy intervals (17.6-Mev incident x-ray energy) and the angular distribution in terms of the electron energy, it is possible to calculate a theoretical energy loss distribution curve for scintillator No. 2 in the following manner. The angle a Compton recoil electron makes with the incident photon is fixed for a given photon energy by the relation²⁵

$$\tan^2 \theta_E = \frac{2\alpha(\gamma/E - 1) - 1}{(1 + \alpha)^2}$$

where γ = energy of incident photon in Mev;

E = energy of recoil electron;

$\alpha = \gamma/mc^2$;

mc^2 = electron rest mass, 0.51 Mev.

The average angle between the direction of motion of a created electron (positive or negative) and of the photon is⁹

$$\theta_0 = \frac{mc^2}{E}$$

where E is the energy of the electron.

APPENDIX I

CALCULATION OF DIFFERENTIAL ENERGY LOSS DISTRIBUTION FOR SCINTILLATOR

NO. 2 AT 17.6-keV INCIDENT X-RAY ENERGY

Using the electron energy distributions given by Johns et al.²⁴ in tabulated form for 1-keV energy intervals (17.6-keV incident x-ray energy) and the angular distribution in terms of the electron energy, it is possible to calculate a theoretical energy loss distribution curve for scintillator No. 2 in the following manner. The angle at Compton recoil electron makes with the incident photon is fixed for a given photon energy by the relation²⁵

$$\cos \theta = \frac{I - (I - \gamma)(1 + \alpha)}{S(1 + \alpha)}$$

where γ = energy of incident photon in keV;

I = energy of recoil electron;

$$\alpha = \gamma/mc^2;$$

mc^2 = electron rest mass, 0.511 MeV.

The average angle between the direction of motion of a recoiled

electron (positive or negative) and of the photon is²⁶

$$\theta_0 = \frac{\cos \theta}{I}$$

where I is the energy of the electron.

Once the electron enters the scintillator, it no longer travels in its initial direction given by ϕ_0 or θ_0 , but is subjected to single and multiple scattering. One method of finding the actual path length of electrons has been discussed by Yang²⁶. Yang uses a correction Δ such that $t' = t + \Delta$, where t' is the actual path length and t is the foil thickness measured in radiation lengths²⁷.

$$\Delta_{\text{average}} = \frac{t^2 E_s^2}{4P^2 \beta^2},$$

where E_s = characteristic energy = 21.2 Mev;

P = electron momentum in Mev;

β = velocity of electron in units of the velocity of light.

This result was derived from the gaussian approximation of Rossi²⁷ but could be obtained from the exact numerical solution of Snyder and Scott²⁸. It is felt that the gaussian approximation is of reasonable accuracy for these calculations and will be used throughout this paper when investigating multiple scattering effects. Using the above formula and the collision loss as a function of energy given in Johns et al²⁴, it was possible to prepare the histogram shown in Figure 9 for the 17.6-Mev lithium gamma-ray.

The Compton cross section at 17.6 Mev was obtained from Davisson and Evans²⁵; but, since the observed pair production cross sections

Once the electron enters the scintillator, it no longer travels in the initial direction given by θ_0 or θ_1 , but is scattered to angles and multiple scattering. The method of finding the actual path length of electrons has been discussed by Yang²⁶. Yang uses a correction Δ such that $t' = t + \Delta$, where t is the actual path length and t' is the full thickness measured in radiation lengths²⁷.

$$\Delta_{\text{average}} = \frac{t_{\text{scat}} + t_{\text{scat}}}{t_{\text{scat}}}$$

where Δ = characteristic energy = 21.5 MeV;
 t = electron momentum in MeV;
 θ = velocity of electron in units of the velocity of light.

This result was derived from the Gaussian approximation of Rossi²⁷ but could be obtained from the exact numerical solution of Snyder and Scott²⁸. It is felt that the Gaussian approximation is

of reasonable accuracy for these calculations and will be used throughout this paper when investigating multiple scattering effects. Using the above formula and the collision loss as a function of energy given in Johns et al.²⁹, it was possible to prepare the histogram shown in Figure 9 for the 19.6-MeV Mithras gamma-ray. The gamma-ray cross section at 19.6 MeV was obtained from Davisson and Evans³⁰, but, since the observed pair production cross section

for lead above 5 Mev differ as much as 10 percent from the calculated values, the value for the pair cross section was the experimental value obtained by Waller²⁹.

The energy loss of the electrons in the converter has not been taken into account in any of the curves shown in Figure 9. Hough³⁰ gives the probability of emission at an angle greater than θ_1 (for large angles) as roughly:

$$\frac{3}{8} \left(\frac{mc^2}{E} \right)^2 \frac{1}{1 - \cos \theta_1}$$

where E is the energy of the observed electron. From this, it can be seen that the actual pair angular distribution will spread the energy loss in scintillator No. 2 out towards the higher energy (longer actual path length). The finite resolution of the photomultiplier will spread the distribution out on both sides of the peak. The resulting qualitative curve is shown in Figure 9.

for lead above 5 Mev differ as much as 10 percent from the calculated

values, the value for the air cross section was the experimental

value obtained by Kalkreuth.

The energy loss of the electron in the converter has not been

taken into account in any of the curves shown in Figure 2. Roughly

gives the probability of emission at an angle greater than θ_1 for

large angles) as roughly:

$$\frac{1}{1 - \cos \theta_1} \left(\frac{2\pi}{\lambda} \right)^2$$

where λ is the energy of the observed electron. From this, it can

be seen that the actual angular distribution will spread the

energy loss in multiplier No. 2 out towards the higher energy

(longer actual path length). The finite resolution of the photo-

multiplier will spread the distribution out on both sides of the

peak. The resulting qualitative curve is shown in Figure 2.

BIBLIOGRAPHY

1. H. W. Koch and R. S. Foote, *Phys. Rev.* 91, 455 (1953).
2. J. L. Burkhardt, Ph.D. Thesis, M.I.T., February 1955.
3. H. W. Koch and R. S. Foote, *Rev. Sci. Inst.* 25, 746 (1954).
4. R. L. Walker and B. D. McDaniel, *Phys. Rev.* 74, 315 (1948).
5. B. B. Kinsey and G. A. Bartholomew, *Can. J. Phys.* 31, 537 (1953).
6. R. R. Carlson et al, *Phys. Rev.* 94, 1311 (1954).
7. J. K. Bair and F. C. Maieschein, *Rev. Sci. Inst.* 22, 343 (1951).
8. S. A. E. Johansson, *Nature* 166, 794 (1950); *Phil. Mag.* (London) 43, 249 (1952).
9. Segre, Experimental Nuclear Physics, Vol. I (1953), John Wiley and Sons (New York).
10. R. K. Swank, *Annual Review Nuclear Science* 4, 111 (1954).
11. T. Hrus and R. B. Day, *Phys. Rev.* 91, 599 (1953).
12. R. L. Walker, *Phys. Rev.* 79, 172 (1950).
13. H. Mark and G. Goldring, Rockefeller Generator Group, M.I.T., private communication.
14. J. G. Campbell and A. J. F. Boyle, *Australian J. Phys.* 6, 171 (1953).
15. W. Heitler, The Quantum Theory of Radiation, Clarendon Press, Oxford (1936).
16. W. A. Fowler and C. C. Lauritsen, *Phys. Rev.* 76, 314 (1949).
17. C. N. Chou, *Phys. Rev.* 87, 376 (1952).

THE ABOLITION

17. C. K. Chou, *Phys. Rev.* **87**, 376 (1952).
16. W. A. Fowler and C. C. Lauritzen, *Phys. Rev.* **76**, 371 (1952).
15. W. Heitler, The Quantum Theory of Radiation, Clarendon Press, Oxford (1950).
14. J. O. Campbell and A. J. F. Boyle, *Australian J. Phys.* **6**, 171 (1953).
13. H. Mark and G. Gollwing, *Weizsaecker Symposium Group*, N.Y.T., private communication.
12. R. L. Waller, *Phys. Rev.* **73**, 175 (1950).
11. T. Huns and R. S. Day, *Phys. Rev.* **91**, 702 (1953).
10. E. K. Swank, *Annual Review Nuclear Science* **4**, 111 (1954).
9. Series, Experimental Nuclear Physics, Vol. I (1953), John Wiley and Sons (New York).
8. S. A. E. Johansson, *Nature* **160**, 791 (1950); *Phil. Mag.* (London).
7. J. K. Bair and F. G. Walsworth, *Rev. Sci. Instr.* **32**, 313 (1961).
6. R. R. Garlick et al., *Phys. Rev.* **91**, 1311 (1954).
5. H. B. Kinsley and G. A. Bartholomew, *Can. J. Phys.* **31**, 537 (1953).
4. R. L. Wether and R. L. McDaniel, *Phys. Rev.* **74**, 315 (1948).
3. H. W. Koch and R. S. Foster, *Rev. Sci. Instr.* **22**, 716 (1951).
2. J. L. Burkhart, Ph.D. Thesis, N.Y.T., February 1955.
1. H. W. Koch and R. S. Foster, *Phys. Rev.* **91**, 1552 (1953).

18. L. Katz and A. S. Penfold, *Revs. Modern Phys.* 24, 28 (1952).
19. Pilot Chemical Company, Waltham, Massachusetts.
20. S. Janes, Synchrotron Laboratory, M. I. T., private communication.
21. K. H. Spring, Photons and Electrons, John Wiley and Sons, New York (1950).
22. R. D. Evans, The Atomic Nucleus, McGraw-Hill, to be published.
23. R. M. Sternheimer, *Phys. Rev.* 88, 851 (1952).
24. H. E. Johns et al, *Nucleonics*, 12, 40 (1954).
25. C. M. Davissen and R. D. Evans, *Revs. Modern Phys.* 24, 79 (1952).
26. C. N. Yang, *Phys. Rev.* 84, 599 (1951).
27. B. Rossi and K. Greisen, *Revs. Modern Phys.* 13, 240 (1941).
28. H. Snyder and W. T. Scott, *Phys. Rev.* 76, 220 (1949).
29. R. L. Walker, *Phys. Rev.* 76, 527 (1949).
30. P. V. C. Hough, *Phys. Rev.* 74, 80 (1949).
31. R. K. Swank and W. L. Buck, *Nucleonics* 10-5, 51 (1952).
32. E. R. Linden, *Nucleonics* 11-9, 30 (1953).
33. J. Saldick and A. G. Allen, *J. Chem. Phys.* 22, 438 (1954).
34. H. A. Bethe and W. Heitler, *Proc. Roy. Soc. (London)*, A46, 83 (1934).
35. L. Eyges, *Phys. Rev.* 77, 81 (1950).
36. E. S. Rosenblum, AECU Report No. 1825 (1951).
37. W. Paul and H. Reich, *Z. Physik* 127, 429 (1950).
38. J. J. S. Chen and S. D. Warshaw, *Phys. Rev.* 84, 355 (1951).
39. Goldwasser et al, *Phys. Rev.* 88, 1137 (1952).

18. I. Kater and A. G. Penfold, *Rev. Modern Phys.* 34, 58 (1962).
19. *Prior Chemical Company, Waltham, Massachusetts.*
20. S. Jarnes, *Synthesizer Laboratory, M. I. T., private communication.*
21. K. H. Spring, *Photons and Electrons, John Wiley and Sons, New York*

(1970).

22. R. D. Evans, *The Atomic Nucleus, McGraw-Hill, to be published.*
23. R. M. Steinbock, *Phys. Rev.* 88, 871 (1952).
24. H. K. Johns et al, *Nucleonics*, 15, 10 (1951).
25. C. M. Davidson and R. B. Evans, *Rev. Modern Phys.* 34, 19 (1962).
26. C. K. Yang, *Phys. Rev.* 84, 893 (1951).
27. B. Rossi and K. Greisen, *Rev. Modern Phys.* 13, 240 (1941).
28. H. Snyder and W. T. Scott, *Phys. Rev.* 76, 530 (1949).
29. R. L. Walker, *Phys. Rev.* 76, 527 (1949).
30. F. V. C. Nye, *Phys. Rev.* 74, 80 (1949).
31. R. E. Shrock and W. L. Bush, *Nucleonics* 10-2, 51 (1952).
32. H. E. Lither, *Nucleonics* 11-2, 30 (1953).
33. J. Seidick and A. O. Allen, *J. Chem. Phys.* 52, 136 (1954).
34. H. A. Bethe and W. Heitler, *Proc. Roy. Soc. (London)*, A40, 83

(1931).

35. L. Hagedorn, *Phys. Rev.* 77, 81 (1950).
36. E. G. Rosenbluth, *ANU Report No. 1822 (1951).*
37. W. Paul and H. Kohn, *J. Phys.* 157, 159 (1950).
38. J. L. E. Chen and S. B. Wurm, *Phys. Rev.* 84, 352 (1951).
39. Goldberger et al, *Phys. Rev.* 84, 1173 (1952).

- 40. L. Landau, J. Phys. USSR) 8, 201 (1944).
- 41. Fano, Nucleonics, 11-8, 8 (1953).

TH-37
S6628

Snyder

28794

Instrumentation and
calibration of X-ray
scintillation pair spectro-
meter.

S6628

Snyder

28794

Instrumentation and
calibration of X-ray scin-
tillation pair spectrometer.

thesS6628

Instrumentation and calibration of x-ray



3 2768 002 00830 2

DUDLEY KNOX LIBRARY